Department of Electrical
and
Computer Systems Engineering

Technical Report
MECSE-7-2005

Photonic Signal Processing - Part I: Analysis and Graphical Representation of Photonic Circuits

Le Nguyen Binh

MONASH
UNIVERSITY

PHOTONIC SIGNAL PROCESSING-PART I: ANALYSIS AND GRAPHICAL REPRESENTATION OF PHOTONIC CIRCUITS

Le Nguyen Binh
Department of Electrical and Computer Systems Engineering,
Monash university, Clayton, Melbourne Victoria 3168 Australia.
e-mail: le.nguyen.binh@eng.monash.edu.au

Abstract:

The fields of photonic communications and integrated photonics have progressed significantly over the last few decades of the 20th century. Spinning off from such developments, several related areas such as microwave photonics, photonic switching etc. have been established. In these systems, photonic signals are propagating and processed at the modulators, through the guided media, at the multiplexers and demultiplexers, through optical amplifiers (Raman, rare-earth doped waveguide or parametric amplification). Thus the necessity of processing of photonic waves has become important and thus requires fundamental approaches for photonic circuit analysis, syntheses and design, the photonic signal processing.

This report, as the first pat of the series for photonic processors, therefore presents the fundamental principles and applications of this new field of photonic signal processing. We state the issues of coherence and incoherence of lightwaves propagation through photonic circuits and hence the representation of lightwaves and circuits either by the lightwave intensity or by the photonic electromagnetic fields. The photonic circuits to be processed in coherent or incoherent modes are described and followed by a number of photonic circuit elements. The graphical representation of photonic circuits is described using the signal flow graphs and the photonic Mason's rules. Automatic generation for photonic transfer functions of the input and output lightwave signals between any two nodes of a photonic circuit are presented.

TABLE OF CONTENTS

TABLE OF FIGURES

1 Introduction

Photonic fiber technology for telecommunications has reached an advanced stage. On the other hand microwave photonics has also attracted attention in the last decade or so. The applications of photonic technology have also been extended to the fields of fiber optic sensors and ultra-fast photonic laser sources. The loss of photonic fibers have been lowered to near the theoretical limits, in fraction of dB per km, and its low dispersion, i.e. a length-bandwidth product of several thousands of GHz-km for single mode fibers, Standard SMF, NZ-DSF etc., has been achieved. Furthermore several advanced photonic elements have also been designed and manufactured with integrated optic or fiber-optic structures. They allow the design of compact photonic processors as the delay length can be shortened to with a unit delay of signal sampled at several Gb/s.

Synthesize and implement several attractive photonic signal processors for photonic computing as well as communications networks. Photonic processors such as photonic filters have an ability to process high speed signals avoiding costly electro-optic (E/O) and opto-electronic (O/E) conversions which eventually create bottlenecks. In order to design photonic processors there needs a systematic technique to represent the signals, the lightwaves and the photonic components which can form processors. This series of articles is addressing the theoretical analyses, design and syntheses and demonstration of photonic processing techniques and systems.

This report is the Part I of the series that present the fundamental issues of coherency and incoherency and circuit representation of photonic circuits as whether we should process the evolution of lightwaves propagation in term of their intensity or electromagnetic fields. The report is organized as follows: Section 2 states the validity of coherent and incoherent lightwaves and their propagation, Section 3 addresses the processing techniques for coherent and incoherent circuits. The graphical signal flow and their transmittance gains are also described in Section 4. A demonstration of the application of the SFG technique for lightwaves propagation

through a number of basic photonic elements and a PSP is illustrated in Section 4.2. Finally conclusion remarks are given.

2 Coherent and Incoherent Photonic Processing

2.1 Coherent and incoherent processing

In this section, the fundamental theory of incoherent and coherent PSP, which provides the basis for later sections, is described. The advantages and disadvantages of incoherent and coherent photonic systems and means of overcoming their limitations are outlined. The characteristics of the fundamental components of incoherent fiber-optic signal processors (see this section) and coherent integrated-optic signal processors are then described

The phase of the photonic signal is sensitive to environmental fluctuations such as temperature and pressure changes and acoustic vibrations as well as frequency fluctuations of the photonic source. The inherently high sensitivity of the photonic phase to environmental effects has made it attractive for sensor applications but unattractive for signal processing operations in which stability is essential. Obviously, these effects can be obviated by discarding the photonic phase through the use of an incoherent light.

Incoherent photonic signal processors require the coherence time of the photonic source to be much shorter than the unit time delay (or sampling period) to avoid undesirable effects of photonic interference. Hence, incoherent systems use intensity variations on photonic carriers for performing signal processing operations. In incoherent systems, single-mode photonic fibers can be used as a promising delay-line medium for processing broadband signals because of the large bandwidth of photonic fibers. Typically, the basic delay-line length[1] of an incoherent fiber-optic signal processor is in the meter-order and is at least several orders of magnitude greater than the coherence length of the photonic source, depending on the frequency of operation. For this reason, changes in the basic delay-line length, due to environmental effects and/or errors in cutting the fiber length, can be tolerated

[1]The basic delay-line length has a delay corresponding to the basic time delay or sampling period of the system.

without causing significant degradation of the system performance. Although incoherent fiber-optic signal processors are stable and robust, they can only perform positive-valued but not bipolar or complex-valued signal processing operations and hence have limited applications. This serious limitation can clearly be overcome with a coherent light if the instability can be found.

In contrast to the incoherent case, coherent photonic signal processors require the coherence time of the photonic source to be much longer than the basic time delay to achieve coherent interference of the delayed signals. Coherent systems are thus capable of performing complex-valued signal processing operations because both the phase and amplitude of the photonic signal are retained in the processed information. As pointed out above, coherent systems cannot operate stably unless the frequency fluctuations of the photonic source and environmental effects can be prevented. The frequency can be stabilized by using highly coherent semiconductor lasers which are commercially available. The environmental effects can be suppressed by using integrated photonic waveguides (instead of photonic fibers) as a comparatively small delay-line medium for broadband signal processing because of their large bandwidth. Coherent integrated-optic signal processors can operate stably because the waveguide length, which is in the cm-order or mm-order, can be accurately fabricated to the precision of the wavelength order and the phase of the photonic signal can be conveniently controlled to the precision of the wavelength order.

In this study, photonic fibers and integrated photonic waveguides or photonic crystals can be considered as the delay-line media of choice for incoherent and coherent PSP, respectively. The fundamental theories of both incoherent fiber-optic signal processing and coherent integrated-optic signal processing are presented in the next sections.

The potentially large bandwidth of photonic fiber has made it an attractive delay-line medium for incoherent processing of broadband signals. This section describes the theory of incoherent fiber-optic signal processing given in references [1-4].

In incoherent photonic signal processors, the information signal (e.g., RF or microwave) to be processed is modulated as intensity variations onto a photonic

carrier whose coherence time is much shorter than the basic time delay in the system. The photonic source can be a broad-linewidth semiconductor laser diode which can be directly modulated at speeds up to several GHz. In the time domain, the modulated wideband signals do not interfere with each other but are appropriately delayed and incoherently combined at the system output. In the frequency domain, the frequency response of the incoherent system depends on the interference of the modulation frequency (RF or microwave) but not the photonic carrier frequency. In other words, an incoherent system is incoherent at the photonic carrier frequency but coherent at the modulation frequency. Thus, the phase of the photonic carrier can be discarded and the signals add on an intensity basis. As a result, incoherent systems are stable and robust but they can only perform positive-valued signal processing operations because intensity cannot be negative, and hence have limited applications. Using the theory of positive systems, it has been shown that the impulse response of an incoherent system is real and positive-valued [1]. In addition, the magnitude of the frequency response of an incoherent system reaches the maximum at the origin of the frequency axis. Consequently, incoherent systems can only be designed to have a limited number of lowpass characteristics but not highpass or bandpass characteristics.

Incoherent fiber-optic signal processing was initiated by the research group at Stanford University in the 1980s [1-4]. Photonic fibers and tunable fiber-optic directional couplers have been used in the analysis, design and construction of a number of incoherent FIR[2] (finite impulse response) and IIR[3] (infinite impulse response) fiber-optic signal processors that can perform a variety of linear signal processing functions. These include convolution, correlation, analog matrix operations, frequency filtering, pulse-train generation, data-rate transformation and code generation. Considerable research effort has produced a number of new concepts, techniques and applications as a result of the advanced development of fiber-optic signal processors [3]–[22]. Photonic amplifiers, in particular erbium-

[2]Note that FIR filters have no feedback loops and are also known as transversal, non-recursive or tapped delay-line filters.
[3]Note that IIR filters have at least one feedback loops and are also known as recursive or re-circulating delay-line filters. All-pole and all-pass filters are special types of IIR filters.

doped fiber amplifiers (EDFAs), have been used to overcome losses as well as to provide greater flexibility in the analysis, synthesis and construction of incoherent fiber-optic signal processors for various filtering applications [7]–[22]. The resulting amplified fiber-optic signal processors have better performances and hence more applications than the non-amplified processors [1]–[6]. Adaptive techniques have also been proposed to provide dynamic weighting of the filter coefficients as well as reconfiguration of the filter delays [4]–[6], [9]–[12].

The limitation of the incoherent (or positive) fiber-optic signal processors may be reduced by using an electronic differential detection scheme, which can have negative filter coefficients but at the expense of increased system complexity [1], [23], [24]. It has been claimed that this synthesis technique can implement not only lowpass filters (LPF) but also highpass (HPF) and bandpass filters (BPF) [23]. The performance of the synthesized filter can only approximate that of the desired filter because the synthesis method is based on the least squares approach. Nevertheless, impressive performances of the synthesized LPF and HPF have been experimentally demonstrated [24]. However, the synthesis technique can only handle bipolar numbers but not complex numbers which must be operated by coherent systems.

It is well known that the basic elements required for implementation of the FIR and IIR digital signal processors are delays, adders and multipliers [25]. As a result, the basic components required for the realisation of the FIR and IIR incoherent fiber-optic signal processors are: fiber-optic delay lines, fiber-optic directional couplers and fiber-optic (or semiconductor) amplifiers. These are described in the following sections.

2.2 Photonic Delay Lines

The output of a delay element is the input delayed by a unit time. This unit of delay can be considered as a sampling period for a discrete-time system. That is, for the input signal discretized-time signal input *f(k)* the output is *f(k-1)* as shown in ***Figure 1***.

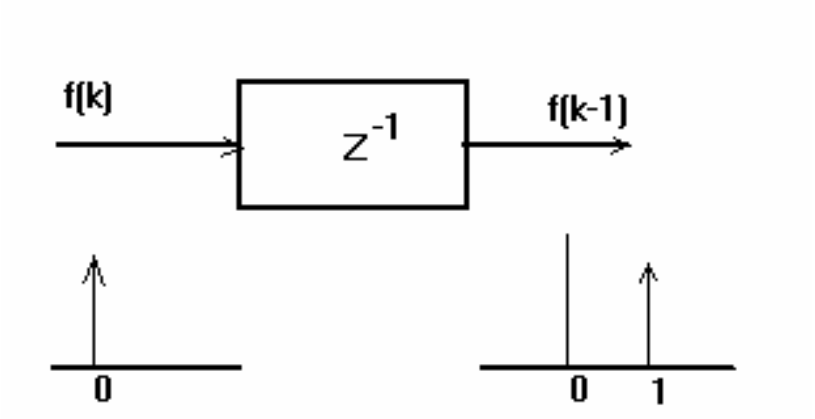

Figure 1 Photonic time delay element using a photonicfiber length L. The unit delay time unit is represented as z^{-1}.

The z^{-1} inside the block diagram represents a unit time delay. The z-transform is used here if we assume that the system is operating under a discretized system. In fact there is a transformation technique that can be used to convert a z-transformed transfer function to a s-domain equivalent. The delay element is the photonic fiber of length L. assuming that the refractive index of a photonic waveguide is n=1.5 at 1.3 μm, then the propagation delay T is given by

$$T = \frac{n\,L}{c} \qquad (1)$$

where c is the velocity of light in vacuum ($3x10^5$ km/s). The propagation delay for the single mode optical fiber is about 5 ns/m. If the signals are sampled at 2.5 ns per bit period then a meter of photonic fiber would correspond to 2 delay units or it can be represented by z^{-2}. Deriving the photonic transfer function (usually called as photonic transmittance in physics) of a photonic network, electromagnetic fields are employed.

Assuming that the input photonic field is E_i and the output photonic field is E_o then the input-output field relationship for a photonic delay element is given by

$$E_o = e^{-\alpha L} e^{-j\beta L} E_i \qquad (2)$$

where α is the photonic field attenuation factor of the photonic fiber; β is the propagation constant of the photonic field propagating along the photonic delay element (photonic fiber); $\beta = k\, n_{eff}$ with $k = 2\pi/\lambda$ and n_{eff} is the effective refractive index of the guided fundamental mode; λ is the photonic wavelength in vacuum. Thus βL represent the phase change of the photonic waves propagating through the fiber length L. Note: α is the field attenuation constant. The normal attenuation constant of a photonic waveguide is referred to intensity, say α_F, then $\alpha_F = 2\alpha$.

Generally if we assign t is the transmission coefficient of the photonic intensity then the field transmission intensity is $t^{1/2}$, (2) can then be written as

$$E_o = t^{1/2}\, e^{-j\beta L}\, E_i \tag{3}$$

Then the transmission coefficient t is less than unity for a photonic waveguide without an in-line photonic amplifier. In case that there is in-line photonic amplifier with a small intensity gain G then (15) can be rewritten as

$$E_o = G^{1/2}\, t^{1/2}\, e^{-j\beta L}\, E_i \tag{4}$$

We assume that the gain G is uniform over the operating wavelength of interest. In case that several photonic wavelength carriers are used then the gains at each of the wavelength region must be specified. Normally erbium doped photonic amplifiers (EDFAs) are used as in-line fiber photonic amplifiers in photonic fiber signal processing system. Unfortunately the gain over the wavelength of interest of 1550 nm with a 40 nm bandwidth is not flat. Thus one must make sure that the gain at the operating wavelength is known.

The low loss and broad bandwidth of optical fibres (photonic waveguides) have made them an attractive delay-line medium for incoherent processing of high-speed broadband signals directly in the photonic domain. The loss of photonic fibers is about 0.5 dB/km at 1300 nm and about 0.2 dB/km at 1550 nm. The bandwidth–distance product of photonic fibers is about 32 THz · km at 1300 nm and about 100 GHz · km at 1550 nm [26]. As a result, the time–bandwidth product of photonic

fibers exceeds 10^7 at 1300 nm and exceeds 10^5 at 1550 nm, assuming a delay per unit length of $5\,\mu s/\text{km}$.

2.3 Photonic tapping and coupling

Various photonic techniques can be used to produce the tapping elements such as evanescent directional couplers, fused photonic couplers. The coupling and tapping can be represented in ***Figure 2***.

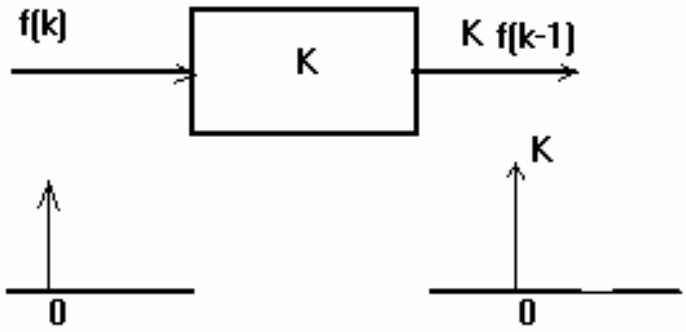

Figure 2 Single input-single output tapping element

The single-input single-output photonic tapping element can be implemented by bending the photonic fiber so that photonic field or energy is leaked out. In this case the intensity tapping coefficient is less than 1 (*K<1)*. The coefficient *K* can be greater than 1 if the tapping element is a photonic amplifier. In this case the tapping coefficient is replaced by a small-signal gain factor G.

Figure 3 shows the block diagram of a 2x2 photonic coupler. The input photonic fields are assigned as E_1 and E_2 and output fields are denoted with E_3 and E_4. These input and output fields are coupled through a coupling coefficient $K^{1/2}$, with K is the intensity coupling coefficient. The coupling matrix is given by

$$\begin{pmatrix} E_3 \\ E_4 \end{pmatrix} = (1-\gamma)^{1/2} \begin{pmatrix} (1-K)^{1/2} & -jK^{1/2} \\ -jK^{1/2} & (1-K)^{1/2} \end{pmatrix} \begin{pmatrix} E_1 \\ E_2 \end{pmatrix} \quad (5)$$

where γ = the excess intensity coupling loss factor of the coupler. The *-j* factor in the above matrix represents a phase shift of $-\pi/2$. This is the characteristics of most photonic couplers.

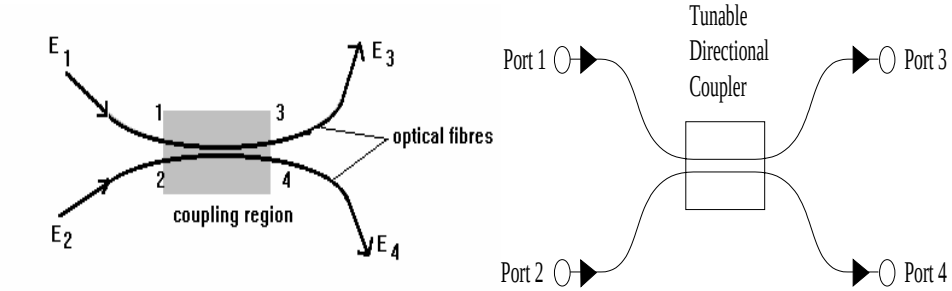

Figure 3 Schematic diagram of a 2x2 photonic coupler (a) generic structure (b) port allocation- intensity dependent.

It is observed that the energy is conserved in the photonic coupler, the matrix satisfies the unitary condition. Using (5) we have:

$$|E_3|^2 + |E_4|^2 = |E_1|^2 + |E_2|^2 \tag{6}$$

provided that the coupling loss is negligible ($\gamma=0$). In case that the coupler is asymmetric then the coupling matrix is given by

$$\begin{pmatrix} E_3 \\ E_4 \end{pmatrix} = (1-\gamma)^{1/2} \begin{pmatrix} a_{11} & a_{12} \\ a_{21} & a_{22} \end{pmatrix} \begin{pmatrix} E_1 \\ E_2 \end{pmatrix} \tag{7}$$

where a_{11}, a_{12}, a_{21} *and* a_{22} are the coupling and cross coupling factors between ports 1,2 and 3,4 respectively. For a photonic coupler fabricated by identical core photonic waveguides then the coupling coefficients are given by

$$a_{11} = a_{22} = (1-\kappa)^{1/2} \qquad \textit{and} \qquad a_{12} = a_{21} = -j\kappa^{1/2} \tag{8}$$

that means that the cross coupling from port 1 to 4 or 2 to 3 results a $\pi/2$ phase shift. This condition is not hold for the case in which the cores of the two waveguides of the coupler are not the same.

Similar to the case of coherent operating regime, the ***intensity*** transfer matrix of a *2x2* tunable photonic directional coupler can be described incoherently by [1]

$$\begin{bmatrix} I_3 \\ I_4 \end{bmatrix} = (\gamma)\begin{bmatrix} 1-\kappa & \kappa \\ \kappa & 1-\kappa \end{bmatrix}\begin{bmatrix} I_1 \\ I_2 \end{bmatrix} \tag{9}$$

where $\{I_1, I_2\}$ and $\{I_3, I_4\}$ are the intensities at the input and output ports, respectively, κ $(0 \le \kappa \le 1)$ is the cross-coupled intensity coefficient, and γ (typically $0.95 < \gamma < 1$) is the intensity transmission coefficient. (9) means that, when the input port $\{2\}$ is not excited, the signal intensity at the input port $\{1\}$ is directly coupled to the output port $\{3\}$ with an intensity coupling coefficient of $\gamma(1-\kappa)$ and cross coupled to the output port $\{4\}$ with an intensity coupling coefficient of $\gamma\kappa$. Similarly, when the input port $\{1\}$ is not excited, the signal intensity at the input port $\{2\}$ is directly coupled to the output port $\{4\}$ with an intensity coupling coefficient of $\gamma(1-\kappa)$ and cross coupled to the output port $\{3\}$ with an intensity coupling coefficient of $\gamma\kappa$.

2.4 Photonic Amplifiers

Photonic amplifiers are devices that amplify the number of photons of a signal to give higher number, thus amplification in photon domain. They can be in the form of rare-earth metal doped fibres, e.g. Er or Nd for 1550 nm or 1000 nm spectral regions respectively, of integrated optic PLC or semiconductor materials. Photonic amplifiers are also a very important photonic component in incoherent fiber-optic signal processors. They can compensate for photonic losses as well as providing design flexibility resulting in potential applications.

Photonic amplifiers can provide signal amplification directly in the photonic domain. The operational principles, characteristics and performances of the photonic amplifiers described here have been obtained from references [26] and [29]. The gain of a photonic amplifier is generated by the processes of stimulated scattering induced by nonlinear scattering in a photonic fiber, or stimulated emission caused by a population inversion in a lasing medium. The former process is utilized by stimulated Raman scattering fiber amplifiers, parametric and stimulated Brillouin scattering (SBS) fiber amplifiers, which are of little interest in this investigation because they

are based on nonlinear effects in fibers. The latter process is employed by semiconductor laser amplifiers (SLAs) or rare-earth doped fiber amplifiers.

Semiconductor lasers can be designed to act as amplifiers and hence the acronym SLAs. SLAs can be categorized, according to biasing condition and structure, into three types: injection-locked (IL), Fabry-Perot (FP), and traveling-wave (TW) SLAs. IL-SLA and FP-SLA, which are based on resonance effects, require the biasing of the semiconductor laser above and below the lasing threshold, respectively. By contrast, TW-SLA, which exploits single-pass amplification, requires both facets of the semiconductor laser to have antireflection coating. Considerable research attention was initially paid to IL-SLA and FP-SLA with a view to improving the inferior antireflection coating methods. However, TW-SLA has recently attracted the most attention because of its superior performance (saturation output, noise and bandwidth, to mention a few) and of considerable progress with coating techniques. However, note that it is difficult to differentiate between FP-SLA and TW-SLA because complete zero reflectivity cannot be easily achieved by actual antireflection coating techniques. Thus, it is generally accepted that TW-SLA and FP-SLA have reflectivity of less than 0.1–1% and more than 30%, respectively. For these reasons, the TW-SLAs have been chosen in this study for application in incoherent fiber-optic signal processors.

The rare-earth doped fiber amplifiers make use of ions such as erbium, neodymium and praseodymium, to name a few, as the gain medium to provide photonic amplification. In recent years, EDFAs using pump lasers at 980 nm or 1480 nm have been commercially available simply because they operate near 1550 nm, the wavelength region in which the fiber loss is minimum and hence the wavelength window of interest for next-generation lightwave systems. For these reasons, EDFAs have also been considered in this investigation.

Because the TW-SLAs and EDFAs are considered in this report, it is necessary to understand their characteristics and performances which are summarized in ***Table 1*** [29]. Compared with TW-SLAs, the advantages of EDFAs are: higher unsaturated (or small-signal) gain, higher saturation output power, lower noise figure, lower fiber coupling loss, and polarization independence. However, TW-SLAs generally have

larger bandwidth and are more compact than EDFAs. The high gain, high saturation output, large bandwidth, low noise, low fiber coupling loss, and polarization independence of EDFAs make them an ideal choice for application in the incoherent fiber-optic signal processors. In addition to the enormous bandwidth and compactness, the relatively fast switching speed of TW-SLAs makes them more attractive than EDFAs for application in adaptive (or programmable) incoherent fiber-optic signal processors, where the gains of the TW-SLAs can be altered by varying the injection current sources driving the semiconductor lasers. Programmable incoherent fiber-optic signal processors incorporating TW-SLAs must use polarization-preserving fibers and couplers because of the polarization dependence of TW-SLAs.

In this report, EDFAs and TW-SLAs have thus been considered as the amplifiers of choice for non-programmable and programmable incoherent fiber-optic signal processors, respectively.

TW-SLAs	Characteristics/performances	EDFAs
Various wavelengths	Signal wavelength	Currently 1550 nm band only
15 ~ 20 dB	Unsaturated gain	40 ~ 50 dB
0 ~ 3 dBm	Saturation output power	10 ~ 20 dBm
> 3 THz	Bandwidth	1 ~ 4 THz
Yes	Polarization dependence	No
6 ~ 9 dB	Noise figure	3 ~ 5 dB
Large loss (9 ~ 10 dB)	Fiber coupling loss	Low loss (< 0.5 dB)
Fast switching (< 1 ns) Short carrier lifetime	Switching speed	Slow switching (0.2 ~ 10 ms) Long carrier lifetime
Small, amplifier length of < 1 mm	Size/length	Several meters to several 100 m of fiber length

Table 1 Comparison of the characteristics and performances of photonic amplifiers[4].

2.5 Coherent Photonic Signal Processing

Integrated photonic waveguides can be used as an attractive delay-line media for coherent processing of ultra-high-speed broadband signals because of the high precision (and hence stability) and large bandwidth of the waveguides. In coherent photonic signal processors, the information signal (RF, microwave or mm-wave) to be processed is impressed onto a photoniccarrier whose coherence time is much longer

than the basic time delay in the system. The photonic source must be a frequency-stabilized highly coherent semiconductor laser with a very narrow linewidth in order to suppress the frequency instability. Thus, the photonic source must be externally (rather than directly) modulated so that its high degree of coherence can be maintained. This is because direct current modulation of the injection lasers causes a dynamic shift of the peak emission wavelength resulting in broadening the spectral width [30]. In addition, external modulation (e.g., using titanium-diffused lithium niobate waveguide modulators) of the photonic source permits high-speed modulation which is ideal for high-speed signal processing. Thus, the use of external modulators allows the photonic source to be optimized for spectral quality as well as obtaining high modulation bandwidth. In the time domain, the modulated signals constructively or destructively interfere with each other, depending on their relative phases. In the frequency domain, the frequency response depends on the interference of the photonic carrier frequency. Thus, coherent photonic signal processors using integrated-optic waveguides can stably perform high-speed complex-valued signal processing operations because both the phase and amplitude of the photonic carrier are retained in the processed information. The use of the photonic modulators have recently attracted attention in generation of novel modulation schemes such as RZ, NRZ, CSRZ, Rz-DPSK, DQPSK for long-haul and high spectral efficient transmission [78]

The term "integrated optics" was suggested by Miller in 1969 at a Bell Laboratory as the lightwave equivalent of "integrated electronics" [31]. Since then research in integrated optics and now in 2005 as "integrated photonics" and "photonic crystals" has begun and gained momentum at about the same time as the development of low-loss photonic fibers and semiconductor lasers. The concept of integrated optics involves the use of thin-film and micro- and nano-fabrication technologies in the development of a large number of individually fabricated miniature photonic components, which may be integrated (or individually interconnected) onto a single chip in a similar fashion to that which had taken place with integrated electronic circuits [31]–[35]. Significant progress has been made in this field with advances in material developments, design techniques, fabrication processes, and component developments. Developments have now reached the stage where integrated photonic

[4] Extracted from [79]

circuits can be realized to perform various PSP and switching functions. Indeed, recent advances in lightwave technology and networks have further accelerated the pace for the development of compact, rugged, stable and economical integrated photonic circuits for flexible processing and switching of high-speed broadband signals directly in the photonic domain.

Integrated PLCs have several advantages over its counterpart, the integrated electronic circuits, or over conventional bulk-optic systems consisting of relatively large discrete components [35]. When compared to bulk-optic systems, integrated PLCs share the same advantages as those of the integrated electronic circuits such as smaller size and weight as well as improved reliability and batch fabrication economy. However, the integrated PLC, which uses a high carrier frequency for information processing, inherently has a higher processing speed than the integrated electronic circuit. As with any other new technology, a high development cost of integrated-optic technology (e.g., developing new fabrication technology) is initially required.

Integrated PLCs can be fabricated on several different materials, each with its own particular features. The choice of a substrate material depends very much on the function to be performed by the circuit. Substrate materials commonly used are glass, $LiNbO_3$, silicon (Si), III–V[5] semiconductors, such as gallium arsenide (GaAs) and indium phosphide (InP) [32]–[35]. For example, the InGaAsP / InP material system has been used for the development of InGaAsP / InP 1.55-μm distributed feedback lasers because the InP substrate is capable of emitting light in the 1.3–1.6 μm spectral region which is important for lightwave systems [36]. The $LiNbO_3$ dielectric material has been widely used for the development of Ti:$LiNbO_3$ waveguide modulators because of its linear electro-optic effect, and that the photonic waveguide can be easily formed by diffusing a thin film of titanium into the $LiNbO_3$ substrate [32]–[35]. The germanium, InGaAs / InP and InGaAsP / InP materials have been used for the fabrication of avalanche photodiodes because of their high absorption coefficients (or responsivity) in the 1.1–1.6 μm low-loss wavelength region [36].

[5]Note that compounds made of elements (e.g., gallium and arsenic) found in the third and fifth columns of the periodic table are called III–V semiconductors.

The fundamental component of any PLC is the photonic waveguide. Compared with waveguides made of other materials, single-mode silica-based waveguides, which have almost the same composition as that of single-mode photonic fibers, are more compatible with photonic fibers and hence have lower fiber coupling loss [37]–[39]. Two major processes have been used for the fabrication of single-mode silica-based waveguides on planar silicon substrates: chemical vapor deposition and flame hydrolysis[6] deposition. The single-mode waveguide patterns are then defined by photolithographic pattern definition processes followed by reactive ion etching. The glass systems commonly used for the silica-based waveguides are: phosphorous-doped silica ($SiO_2 - P_2O_5$) which is formed by chemical vapor deposition [40], and titanium-doped silica ($SiO_2 - TiO_2$) and germanium-doped silica ($SiO_2 - GeO_2$) which are formed by flame hydrolysis deposition [37], [38]. It has been claimed by research groups at NTT Japan laboratories that the combination of flame hydrolysis deposition and reactive ion etching can produce low-loss silica-based waveguides which are best matched to photonic fibers [37], [38]. A variety of passive integrated photonic circuits, which are also known as planar lightwave circuits (PLCs), using single-mode silica-based waveguides on silicon substrates fabricated by a combination of flame hydrolysis deposition and reactive ion etching have been demonstrated as: splitters [37], low-speed photonic switches [37], [41]–[43], photonic wavelength-division muxes or demuxes [37], [44]–[46], photonic frequency-division muxes/demuxes [37], [47]–[50], tunable photonic filters [50]–[52], and photonic dispersion compensators [53], [54].

PLCs can be realized by two different approaches: hybrid integration, where several devices are fabricated on different materials, with each optimized in a given material, and combined on a common substrate, and monolithic integration, where all devices are fabricated on a common substrate [32]–[35]. Although the monolithic integration is economically attractive because mass production of the circuit can be achieved by automatic batch processing, there is no single substrate material which is ideal in all respects, as described above. In recent years, hybrid integration has been considered as a practical and promising approach for combining many desired functions on a

[6]Flame hydrolysis is a method originally developed for fiber pre-form fabrication.

common substrate, and silicon is an ideal substrate material [37], [38], [55]–[59]. The compatibility of silica-based waveguides on silicon with the photonic fibers, the high thermal conductivity of silicon (and hence a good heat sink), and the good mechanical stability of silicon make it an attractive substrate not only for passive PLCs, but also as a platform (or motherboard) for hybrid integration of opto-electronic devices and as the host materials for rare-earth metal for optical amplification [55]. Hybrid integration platforms have been successfully developed to enable the integration of silica-based waveguides and laser diode chips all on the same silicon substrate [55]–[59]. The present challenging task is to incorporate integrated-optic waveguide amplifiers (e.g., using erbium-doped silica-based waveguides [60]–[62]) into the hybrid integration platform to provide greater functionality for next-generation photonic networks. In addition, the well-developed silicon technology in the micro-electronics industry can be applied to the mass production of hybrid integration of opto-electronic devices, such as photonic sources, photonic amplifiers, and photonic PSP circuits.

In this investigation, the integrated photonic circuits are considered for the design of coherent PSP by the use of (i) low-loss single-mode silica-based waveguides embedded on silicon substrates and photonic crystal structures (ii) photonic crystals at nano-scale in which the coupling length, the bending curvature can reach at very miniscule scale, about million times less than photonic devices achieved with conventional PLC technology. However, the methodology and results are applicable to PSPs using other waveguide materials. Similar to the incoherent PSPs described in Section 2.5, the basic components required for the realization of FIR and IIR coherent PSPs are: integrated-photonic delay lines, integrated-photonic phase shifters, integrated-photonic directional couplers and integrated-photonic amplifiers. These are described in the following section.

2.6 Integrated-Photonic Delay Lines

The high precision and stability of the low-loss large-bandwidth single-mode silica-based waveguide on a silicon substrate have made the waveguide an attractive delay-line medium for processing high-speed broadband signals directly in the photonic domain.

The minimum curvature (or bending) radius[7], the propagation loss of the waveguides and the waveguide-fiber coupling loss are very important characteristics in designing and fabricating PLCs. For high relative refractive index difference between the core and cladding (Δ), the waveguides have the advantage of having a small curvature radius but at the expense of having a large propagation loss and a large fiber coupling loss [37], [49]. In recent years, the $SiO_2 - GeO_2$ waveguide has been preferred to the $SiO_2 - TiO_2$ waveguide because the former glass system has a lower propagation loss. The discussion here is thus focused on the $SiO_2 - GeO_2$ waveguides.

Typically, $SiO_2 - GeO_2$ waveguides with a core of $8 \times 8\mu m^2 \sim 6 \times 6\mu m^2$ and a low Δ of $0.25 \sim 0.75\%$ have a minimum curvature radius of $25 \sim 5$ mm and a propagation loss of less than 0.1 dB/cm [49]. However, high-Δ waveguides ($\Delta = 1.5\%$) with a core of $4.5 \times 4.5\mu m^2$ have a minimum curvature radius of 2 mm, a low propagation loss of 0.073 dB/cm and a fiber coupling loss of 0.9 dB [49]. The small curvature radius of high-Δ waveguides makes it possible to fabricate circuits with curvatures and hence permits high-density integration of circuits. For example, ring resonators require a small ring radius to have a large free spectral range [49], [50]. However, high-Δ waveguides are disadvantageous in terms of poor coupling with conventional single-mode fibers because of the mismatch between their photonic mode fields. This problem can be solved by using mode-field converters by means of a thermally expanded core technique. For example, the coupling loss was reduced from 2.0 dB to 0.9 dB when thermally expanded core waveguides were used [49].

The stress-induced birefringence of the waveguide, which is caused by the difference between the thermal expansion coefficients of the silica glass layers and the silicon substrate, is unavoidable in the fabrication of PLCs. The waveguide birefringence can be eliminated by using either polarization mode converter with polyimide half-wave plate [63] or the laser trimming method [37], [49].

[7]The minimum curvature radius of the waveguide is the radius above which the bending loss is negligible.

2.7 Photonic Phase Shifters

A thermo-optic phase shifter (PS), which utilizes the thermo-optic effect to change the phase of the photonic carrier, is an important element in PLCs because it provides an extra degree of freedom in circuit design [37].

The thermo-optic PS, which consists of a thin film heater placed on the silica waveguide, is based on the temperature dependence of the refractive index of the waveguide. When an electric voltage is applied to the thin film heater, the refractive index of the heated waveguide increases, thus changing the photonic path length by $(dn/dT)L\Delta T$ where $dn/dT = 1\times10^{-5}$ is the thermo-optic constant of silica waveguide, L is the heated waveguide length and ΔT is the temperature increase. For example, when a 5-mm long waveguide is heated by 30°C, the photonic path length changes by 1.5 μm which corresponds to a phase shift of 2π for a 1.5-μm lightwave [64].

2.8 Photonic Couplers

One of the fundamental elements in PLCs is an integrated-photonic waveguide directional coupler, which performs signal collection (or addition) or signal distribution (or tapping). It is thus useful to mathematically characterize both the non-tunable and tunable directional coupler. For analytical simplicity, the insertion loss, propagation delay and waveguide birefringence of the directional coupler are not considered. The electric-field transfer matrix of the lossless non-tunable waveguide directional coupler (the left directional coupler (DC) of ***Figure 4***) can be described coherently by [65]

$$\begin{bmatrix} \overline{E}_1 \\ \overline{E}_2 \end{bmatrix} = \begin{bmatrix} \sqrt{1-k} & -j\sqrt{k} \\ -j\sqrt{k} & \sqrt{1-k} \end{bmatrix} \begin{bmatrix} E_1 \\ E_2 \end{bmatrix} \tag{10}$$

where $\{E_1, E_2\}$ and $\{\overline{E}_1, \overline{E}_2\}$ are, respectively, the electric-field amplitudes at the input and output ports of the left DC, k $(0 \le k \le 1)$ is the cross-coupled intensity coefficient, and $j = \sqrt{-1}$. Equation (2.2) means that, when the input port $\{2\}$ is not excited (i.e., $E_2 = 0$), the input lightwave E_1 is directly coupled to the output port $\{\overline{1}\}$ with an

amplitude coupling coefficient of $\sqrt{1-k}$ and cross coupled to the output port $\{\bar{2}\}$ with an amplitude coupling coefficient of $-j\sqrt{k}$. Similarly, when the input port $\{1\}$ is not excited (i.e., $E_1 = 0$), the input lightwave E_2 is directly coupled to the output port $\{\bar{2}\}$ with an amplitude coupling coefficient of $\sqrt{1-k}$ and cross coupled to the output port $\{\bar{1}\}$ with an amplitude coupling coefficient of $-j\sqrt{k}$. Note that the cross-coupled lightwave experiences a $-\pi/2$ phase shift.

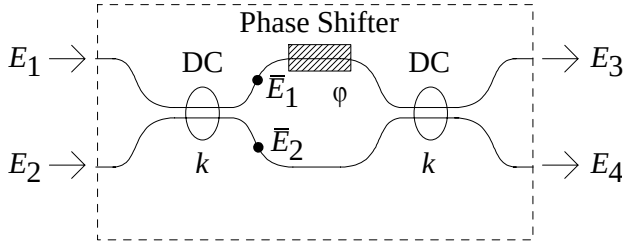

Figure 4 Schematic diagram of the symmetrical Mach-Zehnder interferometer which is used as a tunable coupler (TC). DC represents the non-tunable directional coupler[8].

The fixed coupling coefficient of the non-tunable DC restricts its application in some PLCs. Another disadvantage is that it is difficult to fabricate the non-tunable DC with a precise coupling coefficient. This problem can be overcome by using the symmetrical Mach-Zehnder interferometer (see ***Figure 4***), which can be designed to operate as a tunable coupler (TC) or a photonicswitch [64]. The TC consists of two identical non-tunable DCs interconnected by two waveguide arms of equal length. A thermo-optic PS (see Section 2.7) placed on the upper arm induces a phase shift of φ.

When the input port $\{2\}$ is not excited (i.e., $E_2 = 0$) and using (2), the transfer functions are given by

$$\left.\frac{E_3}{E_1}\right|_{E_2=0} = \sqrt{\gamma_w}\left[\sqrt{1-k}\cdot\exp(j\varphi)\cdot\sqrt{1-k} - j\sqrt{k}\cdot -j\sqrt{k}\right] = \sqrt{\gamma_w}\left[(1-k)\exp(j\varphi) - k\right], \tag{11}$$

[8] Extracted from [79]

$$\left.\frac{E_4}{E_1}\right|_{E_2=0} = \sqrt{\gamma_w}\left[\sqrt{1-k}\cdot\exp(j\varphi)\cdot -j\sqrt{k} - j\sqrt{k}\cdot\sqrt{1-k}\right]$$
$$= -j\sqrt{\gamma_w}\sqrt{k(1-k)}\left[1+\exp(j\varphi)\right], \tag{12}$$

where $\exp(j\varphi)$ is the phase shift factor of the PS and γ_w (typically $\gamma_w = 0.89$ for an insertion loss[9] of 0.5 dB) is the intensity transmission coefficient of the waveguide TC. Similarly, when the input port $\{1\}$ is not excited (i.e., $E_1 = 0$), the transfer functions are given by

$$\left.\frac{E_3}{E_2}\right|_{E_1=0} = \left.\frac{E_4}{E_1}\right|_{E_2=0} \tag{13}$$

$$\left.\frac{E_4}{E_2}\right|_{E_1=0} = \sqrt{\gamma_w}\left[\sqrt{1-k}\cdot\sqrt{1-k} - j\sqrt{k}\cdot\exp(j\varphi)\cdot -j\sqrt{k}\right]$$
$$= \sqrt{\gamma_w}\left[(1-k) - k\exp(j\varphi)\right]. \tag{14}$$

By simple algebraic manipulation of (3)–(6), the electric-field transfer matrix of the TC, which was proposed by Ngo *et al*. [66], is given by

$$\begin{bmatrix} E_3 \\ E_4 \end{bmatrix} = \sqrt{\gamma_w}\begin{bmatrix} \sqrt{1-K}\exp(j\theta_{31}) & \sqrt{K}\exp(j\theta_{32}) \\ \sqrt{K}\exp(j\theta_{32}) & \sqrt{1-K}\exp(j\theta_{42}) \end{bmatrix}\begin{bmatrix} E_1 \\ E_2 \end{bmatrix} \tag{15}$$

where

$$K = 2k(1-k)(1+\cos\varphi), \tag{16}$$

$$0 \le K \le 4k(1-k) \quad \text{or} \quad 0.5 - 0.5\sqrt{1-K} \le k \le 0.5 + 0.5\sqrt{1-K}, \tag{17}$$

$$\theta_{31} = \tan^{-1}\left[\frac{\sin\varphi}{\cos\varphi - k/(1-k)}\right], \tag{18}$$

$$\theta_{32} = -\tan^{-1}\left[(1+\cos\varphi)/\sin\varphi\right], \tag{19}$$

[9]Note that the insertion loss including fiber coupling loss is 0.8 dB [64].

$$\theta_{42} = \tan^{-1}\left[\frac{\sin\varphi}{\cos\varphi - (1-k)/k}\right]. \qquad (20)$$

In (7)–(12), (E_3, E_4) are the output electric-field amplitudes of the TC, K is the cross-coupled intensity coefficient of the TC, and θ_{nm} is the effective phase shift from the input port m to the output port n of the TC. The maximum value of K is $K = 1$ which only occurs at $k = 0.5$ according to (9). It is thus preferable to design both the non-tunable DCs with $k \cong 0.5$ in order to maximize the dynamic tuning range of the TC which is $0 \le K \le 1$. Note that $k = 0.5$ results in $\theta_{31} = \theta_{32} = \theta_{42}$, which implies that the TC is a symmetrical and reciprocal device. For the effective intensity coupling coefficient and the effective phase shifts of the TC for $k = 0.5$ and $0 \le \varphi \le 2\pi$ it can be shown that $0 \le K \le 1$ and $-\pi/2 \le \theta_{31}, \theta_{32}, \theta_{42} \le +\pi/2$ for $0 \le \varphi \le 2\pi$, and that the same value of K occurs at two different values of φ because of the periodicity of K.

Note that it is difficult to precisely fabricate 3-dB ($k = 0.5$) non-tunable DCs, which are important for photonic communication or sensor systems. However, this problem can be overcome by using the TC which can be made exactly 3 dB ($K = 0.5$) provided that $0.1464 \le k \le 0.8536$ [see (9)].

The TC can behave as a photonicswitch when $k = 0.5$ and $\varphi \in (0, \pi)$ [37], [64]. When no electric power is applied to the PS ($\varphi = 0$, off state), the input signals are cross-switched according to the paths: $(1 \to 4,\ 2 \to 3)$. With electric power corresponding to a phase shift of $\varphi = \pi$ is applied (on state), the input signals are direct-switched according to the paths: $(1 \to 3,\ 2 \to 4)$. Typically, the power required for switching is about 0.5 W and the response time is about 1 ms [64]. The response is shown in ***Figure 5***. Alternatively the phase variation can be induced by nonlinear self-phase modulation effects by pumping the photonic section with high intensity light source.

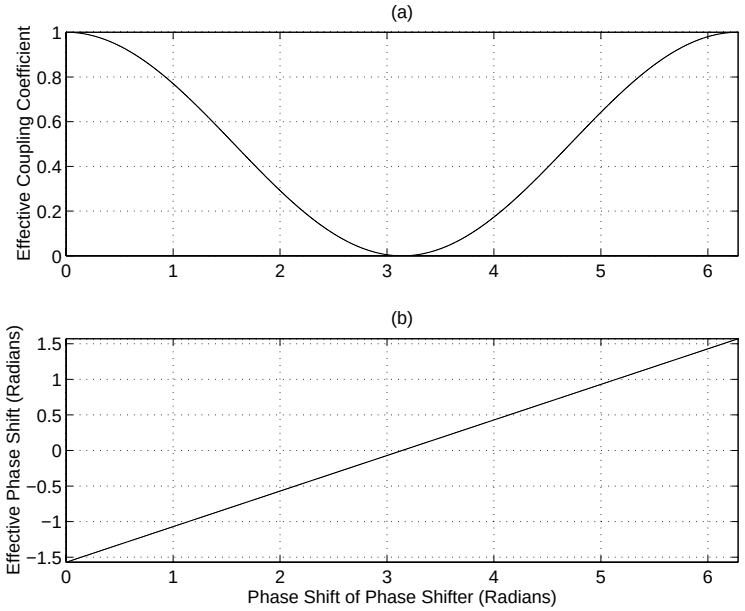

Figure 5 Output responses of the tunable photonic coupler (TOC) for k=0.5 and $0<\varphi<2\pi$ (a) Intensity coupling coefficient K. (b) Effective phase shifts $\theta_{31}=\theta_{32}=\theta_{42}$.[10]

The TOC can operate stably against temperature variation because its operating condition is hardly influenced by environmental temperature change [37]. This is because it is the temperature difference between the two waveguide arms, but not the absolute temperature of each arm, that is important for tunable or switching operation.

2.9 Integrated-Photonic Amplifiers

Integrated-photonic waveguide amplifiers are important active elements for loss compensation as well as for providing design flexibility of PLCs. The resulting amplified PLCs can perform functions which are otherwise not available with the non-amplified PLCs.

A 50 cm - long erbium-doped silica-based waveguide amplifier integrated with a WDM coupler has been successfully demonstrated with a gain of 27 dB, a low noise figure of 5 dB, and a saturated output power of 4.4 dBm [61]. In order to fully integrate amplifier devices with other components on the same chip, the length of the amplifying waveguide must be as short as possible. This can be achieved by increasing the doping level of erbium concentration as much as possible. However, it

[10] See ref. [79]

is believed that there have been no reports to date of experimental results of waveguide amplifiers integrated on PLCs. With recent success in PLC technology, it would not be surprising that PLCs integrated with waveguide amplifiers (or semiconductor amplifiers) become a reality in the next few years. In this research, PLCs using erbium-doped silica-based waveguide amplifiers have thus been proposed as active functional photonic devices for photonic communication systems.

2.10 Remarks

The fundamental theories of incoherent PSP and coherent integrated-photonic signal processing have been described. The major points that can be drawn from this section are given below.

2.10.1Incoherent Photonic Signal Processing

- Incoherent PSPs require the coherence time of the photonic source to be much shorter than the basic time delay in the system, and can be directly or externally modulated.

- In incoherent PSPs the low loss and large bandwidth of the single-mode photonic fiber have made it an attractive delay-line medium for processing broadband signals directly in the photonic domain.

- The characteristics of the fundamental photonic elements (such as photonic delay lines, directional couplers, and photonic amplifiers) of the incoherent PSPs have been described.

- Although incoherent PSPs are stable and robust, they can only perform positive-valued signal processing operations and thus have limited applications. They can process RF and microwave signals with speed ranging from hundreds of megahertz to a few gigahertz because the basic filter length typically ranges from a few meters to tens of meters depending on the frequency of operation.

- The fundamental theory of incoherent PSP described in this section is used in the analysis and design of incoherent PSPs which are presented in the other parts of the series.

2.10.2Coherent PSP

- Coherent integrated-optic signal processors require the coherence time of the photonic source to be much longer than the basic time delay in the system. The photonic source must be a frequency-stabilized highly coherent semiconductor laser which must be externally modulated.

- In coherent integrated-optic signal processors, the high precision and stability of the low-loss large-bandwidth single-mode silica-based waveguide on a silicon substrate have made the waveguide an attractive delay-line medium for high-speed processing of broadband signals directly in the photonic domain.

- The characteristics of the fundamental integrated-optic elements (such as integrated-optic delay lines, integrated-optic phase shifters, integrated-optic directional couplers, and integrated-optic amplifiers) of the coherent integrated-optic signal processors have been described.

- Coherent integrated-optic signal processors can stably perform complex-valued signal processing operations and thus have potential applications in photonic communication systems. They can process mm-wave signals with speed in the range of tens of gigahertz because the basic filter length typically ranges from a few millimeters to a few centimeters depending on the frequency of operation.

- The fundamental theory of coherent integrated-optic signal processing described in this section is used in the analysis and design of coherent integrated-optic signal processors which are presented in other parts of the series.

Note that the choice between an incoherent and a coherent photonic signal processor depends on the particular application.

3 A Simple PSP

A number of basic photonic elements such as photonic couplers, photonic fibers as photonic delay lines, photonic amplifiers, photonic switches, photonic modulators etc have been described in previous section. This section gives an example of a photonic signal processor, the resonator as a system consisting of a coupler and a re0circulaating feedback delay line.

A basic photonic fiber resonator is shown in ***Figure 6***. It consists of a 2x2 photonic fiber or integrated photonic coupler and a positive feedback photonic path from port 3 to port 1 of the 2x2 coupler. The photonic fiber or photonic waveguide feedback has a length *L*.

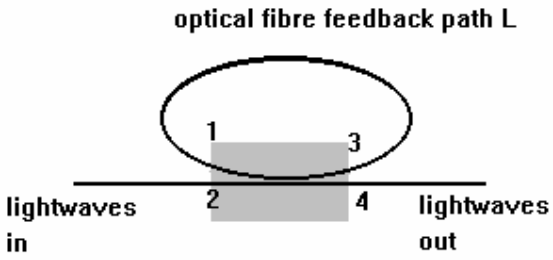

Figure 6 Schematic diagram of a photonic resonator

This photonic fiber resonator is operating under resonance condition when the total phase in the feedback and ring is a multiple number of 2π. This photonic resonator type is called the Fiber Ring Resonator because the fiber feedback configuration forms a ring. Another simple photonic fiber resonator is the Loop Resonator where the photonic feedback path is connected between port 3 and 2 of the 2x2 coupler as shown in ***Figure 7***.

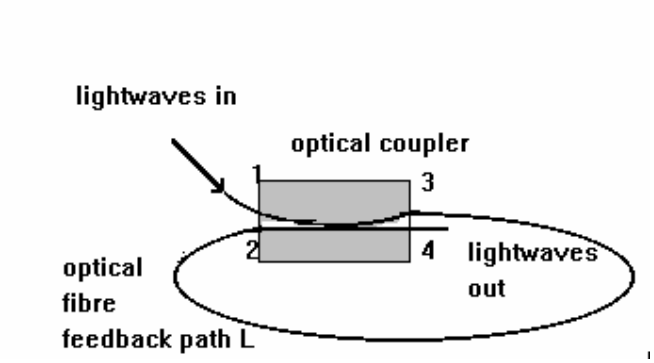

Figure 7 photonic loop resonator. A photonicfiber directional coupler with four ports 1,2,3 and 4. The output port 3 is feedback to port 2 with lightwaves input at port 1.

The field transmittance relationship, and hence obtain the resonance conditions for these two resonators, between the output and input lightwaves of the photonic fiber resonators shown in Figure 1.4 and 1.5 can be obtained as follows: the resonance conditions for the photonic resonator can be obtained by obtaining the relation between the output field E_4 and input field E_1; alternatively the field relationship between the circulating field around the feedback loop E_3 and the input field E_1. The resonator is in resonance if the output field E_4 is depleted while the circulating field is at maximum.

From (17) we have:

$$E_4 = (1 - K)^{1/2} E_1 - j K^{1/2} E_2 \tag{21}$$

and E_2 is related to E_3 by the delay equation (15) i.e.

$$E_2 = t^{1/2} e^{-j\beta L} E_3 \tag{22}$$

with L is the length of the fiber feedback loop. Using (17) again with

$$E_3 = -jK^{1/2} E_1 + (1-K)^{1/2} E_2 \tag{23}$$

Substituting E_2 above to E_3 we obtain the circulating field E_3 as a function of E_1 as

$$\frac{E_3}{E_1} = \frac{(1-K)^{1/2}}{1 + jK^{1/2}\, t^{1/2}\, e^{j\beta L}} \tag{24}$$

thus we have a relationship between E_2 *and* E_1

$$\frac{E_2}{E_1} = \frac{(1-K)^{1/2}\, t^{1/2} e^{j\beta L}}{1 + jK^{1/2}\, t^{1/2}\, e^{j\beta L}} \tag{25}$$

Now substituting E_2 as a function of E_1 *in* E_4 above we have

$$\frac{E_4}{E_1} = \frac{-jK^{1/2} + t^{1/2}\, e^{j\beta L}}{1 + jK^{1/2}\, t^{1/2}\, e^{j\beta L}} \tag{26}$$

or

$$\frac{E_4}{E_1} = \frac{t^{1/2} \cos\beta L + j\,(t^{1/2} \sin\beta L - K^{1/2})}{1 + jK^{1/2}\, t^{1/2}\, e^{j\beta L}} \tag{27}$$

From (27) we can derive the resonance condition for the photonic resonator. It is at resonance when the E_4 approaches 0 that is the real and imaginary parts of (27) must be zero leading to two conditions:

$$\cos\beta L = 0 \quad , or\ \beta L = (2m - 1)\frac{\pi}{2} \tag{28}$$

and $K = t$ (with $\sin\beta L = 1$). These conditions imply that to obtain a good photonic fiber resonator one must design and implement the photonic fiber feedback path so that the total phase of the lightwaves transmitted is a multiple number of $\pi/2$ and the photonic fiber directional coupler must have a coupling constant nearly equal to the transmission coefficient. This transmission coefficient must be close to unity so that there is no energy loss in the resonator.

Practically it implies that one must able to control the fiber feedback length closed to a quarter of an optical wavelength, i.e. about 0.43 μm for 1.3 μm photonic wavelength. What a control. In addition the second condition for resonance states that the coupler coupling constant K must be close to unity. That means that we must be able to fabricate a photonic directional coupler with a coupling coefficient of, say, 99%. The above two conditions must be met in practice

So far we have present only two very basic photonic elements for signal processing and a photonic resonator using passive photonic directional coupler and a feedback photonic fiber path. The derivation for the output and circulating field is based on the field relation between each photonic path. If the number of photonic couplers increases to form more complicated photonic resonators then this derivation technique is inefficient and very tedious. In practice one would prefer to design a photonic resonator so that the stringent requirements for the coupling coefficients are not high. That is neither reaches unity nor to zero. To proceed further with these photonic resonators we should resort to some circuit theory techniques in electrical engineering. This would be outlined in the next section.

4 Signal-Flow Graph Representation for PSP

In this section, a framework for the analysis of photonic signal processors through the application of the signal-flow graph technique is developed as a mathematical tool for later parts. The limitations of other techniques for the analysis of these processors are addressed in Section 3.1. Section 3.2 describes the fundamental theory of the signal-flow graph approach whose effectiveness is then demonstrated by applying it to the analysis of an incoherent recursive PSP (RPSP), as outlined in Section 4.2. Two designs of the incoherent RPSP and their applications as photonic filters are also presented. The theory of incoherent fiber-optic signal processing described in Section 2 is employed in this section where intensity-based signals are considered.

4.1 Photonic Signal-Flow Graph Theory

4.1.1Introductory remarks

A linear time-invariant photonic signal processor is often characterized by its transfer function(s). The analysis and design of photonic signal processors thus require the analysis of their transfer functions which have been obtained by the method of successive substitutions of simultaneous equations [17]–[20] and the transfer matrix method [1], [67]. However, these methods can be tedious, time-consuming and error-prone especially when dealing with a large-scale system, and do not provide a clear picture of the mechanisms in which an input signal flows through (or reflects from) the system.

These problems can be overcome by the use of the signal-flow graph technique proposed in references [68] and [69], which was applied to optics by Binh *et al*. [70]–[72]. References [70]–[72] were concerned with the application of the signal-flow graph technique whose fundamental theory was, however, not given. In this section, the fundamental theory as well as the application of the signal-flow graph method is presented in a more comprehensive manner so that the underlying principles can be easily understood and applied.

A signal-flow graph is defined as a network of directed branches which connect at nodes [68], [69] and is simply a pictorial representation of the simultaneous algebraic equations describing a system and graphically displays the flow of signals through a system. The signal-flow graph method can be interpreted as a transformation of either the method of successive substitutions of simultaneous equations or the transfer matrix method to a topological approach. Thus, it may be said that "a graph is worth a thousand equations" which is analogous with the common saying that "a picture is worth a thousand words". The signal-flow graph technique has been widely used with great success in the diverse fields of electronics, digital signal processing and control systems since its development by Mason in the 1950s [68], [69]. In general, the signal-flow graph theory can be applied to any linear time-invariant systems.

The advantages of the signal-flow graph technique over conventional methods are: it yields a pictorial representation of the flow of signals through the system, which enhances an understanding of the system operation; it provides an easy and systematic way of manipulating the variables of interest, which allows graphical simulation of the system using a computer program [73]; it enables solutions to be easily obtained by direct inspection of simple systems; it permits the identification of the physical behavior and topological properties of a system.

In general, the signal-flow graph technique is used to solve a set of linear algebraic equations, which can be described by [68]

$$x_j = \sum_{i=1}^{n} t_{ij} x_i, \qquad j = 2,3,\cdots,n, \tag{29}$$

where x_1, the only driving force in the system, is the independent variable, $x_2, x_3, \cdots, x_n$ are the dependent variables, and t_{ij} is the transmittance.

4.1.2Definitions of SFG Elements

To understand the signal-flow graph technique, definitions of the fundamental elements of a signal-flow graph [74] are given below.

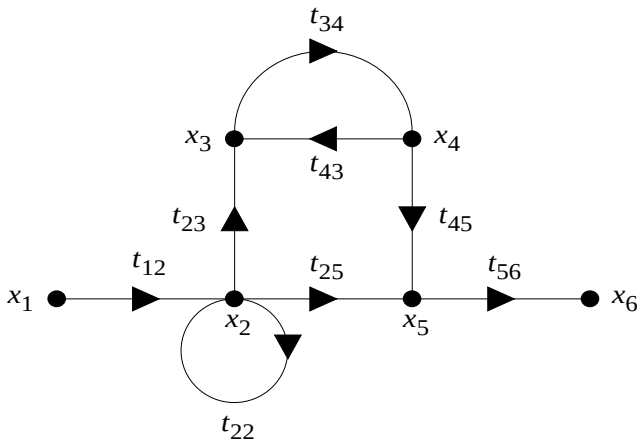

Figure 8 Example of a signal-flow graph.

Definition 1: Photonic node

A photonic **node** (•) represents a variable at which either it generates or receives lightwave or interconnecting lightwaves to and from other photonic nodes.

Definition 2: Photonic branch

A photonic **branch** is a directed photonic path joining two photonic nodes, its direction is indicated by an arrow and its transmittance is specified by an attached symbol (or numeral) describing the functional relation between the two nodes. For example, the symbol $x_1 \rightarrow x_2$ represents a branch which has a transmittance t_{12}.

Definition 3: Photonic source node

A **source node** is a photonic node at which all photonic branches are directed outward. For example, x_1 is a source node.

Definition 4: photonic sink node

A **sink node** is a node at which all photonic branches are directed inward. For example, x_6 is a sink node.

Definition 5: photonic feedback path

A **feedback loop** is a closed path which starts and terminates at the same node such that the nodes can only be touched once per traversal. For example, $x_3 \to x_4 \to x_3$ is a feedback loop.

Definition 6: Photonic self loop

A **self-loop** is a feedback loop consisting of a single branch. For example, $x_2 \to x_2$ is a self-loop.

Definition 7: Photonic non-touching loop

Non-touching loops are separated loops which have no node in common. For example, $x_2 \to x_2$ and $x_3 \to x_4 \to x_3$ are non-touching loops.

Definition 8: Photonic lopp gain

A **loop gain** is given by the product of all transmittances associated with a feedback loop. For example, $t_{34}t_{43}$ is the loop gain of the feedback loop $x_3 \to x_4 \to x_3$.

Definition 9: Photonic forward path

A **forward path** is a path which has no feedback loop and consists of at least one branch. For example, $x_1 \to x_2 \to x_5 \to x_6$ and $x_1 \to x_2 \to x_3 \to x_4 \to x_5 \to x_6$ are forward paths.

Definition 10: Photonic forward path gain

A **forward-path gain** is given by the product of all transmittances associated with a forward path. For example, $t_{12}t_{25}t_{56}$ is the forward-path transmittance gain of the forward path $x_1 \to x_2 \to x_5 \to x_6$.

For clarity, it is preferable to add an additional branch with a transmittance of unity to the source node and to the sink node. ***Figure 9*** shows an example of the equivalence of two graphs where $x_0 = x_1$ is the source node and $x_7 = x_6$ is the sink node.

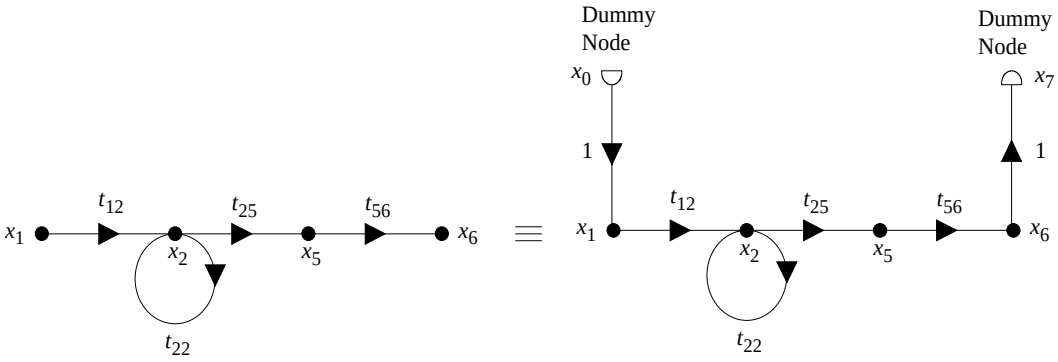

Figure 9 Example showing the equivalence of two signal-flow graphs.

4.1.3Rules of Photonic Signal-Flow Graph

The following basic rules, namely, the transmission, addition and product rules are frequently used in signal-flow graph theory [74].

Rule 1: The Transmission Rule

The value of the variable denoted by a node is transmitted on every branch leaving that node. This can be mathematically described by

$$x_j = t_{ij} x_i, \qquad j = 1, 2, \cdots, n \tag{30}$$

and graphically represented by ***Figure 10***.

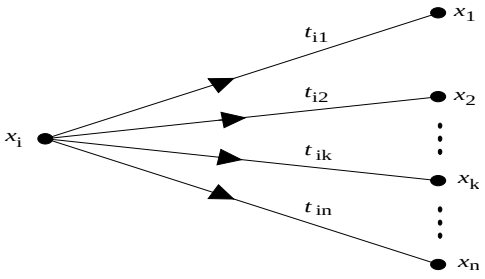

Figure 10 Signal-flow graph representation of the transmission rule.

Rule 2: The Addition Rule

The value of the variable denoted by a node is equal to the sum of all signals entering that node. This can be mathematically described by

$$x_j = \sum_{i=1}^{n} t_{ij} x_i \tag{31}$$

and graphically represented by ***Figure 11***.

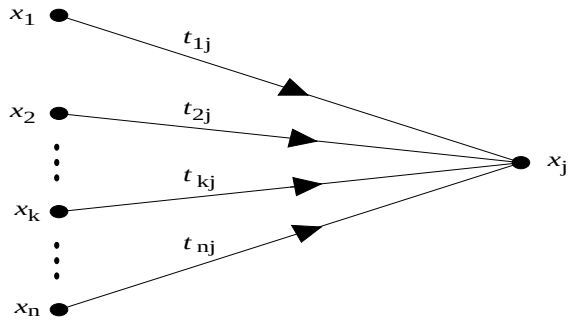

Figure 11 Signal-flow graph representation of the addition rule.

Rule 3: Product Rule

The effective transmittance of a branch is equal to the product of the transmittances of all branches in cascade. This can be mathematically described by

$$x_n = (t_{12} t_{23} \cdots t_{(n-1)n}) x_1 \tag{32}$$

and graphically represented by ***Figure 12***.

Figure 12 Signal-flow graph representation of the product rule.

4.1.4Mason's photonic gain formula

The transfer function H between the independent (or source) node j and the dependent (or sink) node k in the signal-flow graph is determined using Mason's gain formula [74]:

$$H = \frac{1}{D}\sum_{i=1}^{N} P_i D_i \tag{33}$$

where $N =$ the total number of forward paths from node j to node k; $P_i =$ the ith forward-path gain of the forward path from node j to node k; $P_{mr} =$ the mth possible product of r non-touching loop gains; D is the signal-flow graph determinant or characteristic function and is given by

$$D = 1-(-1)^{r+1}\sum_{m}\sum_{r} P_{mr} = 1-\sum_{m} P_{m1}+\sum_{m} P_{m2}-\sum_{m} P_{m3}+\cdots \tag{34}$$

$=$ 1 – (sum of all loop gains) + (sum of all gain-products of 2 non-touching loops) – (sum of all gain-products of 3 non-touching loops) + ⋯;

$D_i =$ the co-factor of the ith forward path $= D$ evaluated with all loops touching P_i eliminated.

The application of (34) is considerably simpler than it appears and is illustrated in Section 4.2.

4.2 An Incoherent Recursive PSP (RPSP)

As an example, the SFG method is applied to the analysis of the incoherent RPSP.

4.2.1Graphical representation

Figure 13 shows the schematic diagram of the incoherent RPSP, which consists of a photonicfiber loop interconnected by two tunable fiber-optic directional couplers DC1 and DC2. The couplers are assumed to have the same intensity transmission

coefficient γ and cross-coupled intensity coefficients κ_1 and κ_2. The signal intensities at the input and output ports are described by $\{I_1, I_8\}$ and $\{I_2, I_7\}$, respectively.

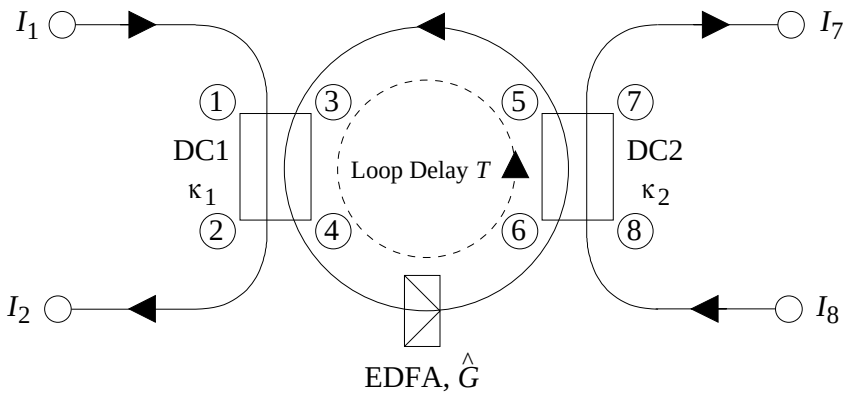

Figure 13 Schematic diagram of the incoherent RPSP. Numbers in circles denote the port numbers of the couplers[11].

The photonic transmittances of the lower (Λ_1) and upper (Λ_2) halves of the ring are defined as

$$\Lambda_1 = G\exp(-j\omega T_1), \tag{35}$$

$$\Lambda_2 = \exp(-j\omega T_2), \tag{36}$$

$$G = \hat{G}\exp[-2\alpha(L_1 + L_2) - 2(\varepsilon_1 + \varepsilon_2)]. \tag{37}$$

In (3.6), G is the effective photonic loop gain, $\hat{G}$ is the intensity gain of the erbium-doped fiber amplifier (EDFA) which has been described in Section 2.4, α is the amplitude attenuation coefficient of the fiber, ε_1 and ε_2 are the amplitude coefficients of the splice (or connector) losses of the lower and upper halves of the ring, respectively, $j = \sqrt{-1}$, ω is the angular modulation frequency, L_1 and L_2 are the fiber lengths of the lower and upper halves of the ring, respectively, and T_1 and T_2 are the corresponding time delays of the lower and upper halves of the ring, respectively. Note that the lengths of the lower and upper halves of the ring do not necessarily need

[11] extracted from [79]

to be the same. It is the fiber loop length $L = L_1 + L_2$ or loop delay $T = T_1 + T_2$ that is important for signal processing.

As a representative value, the exponential factor in (36), which represents the fiber loop loss, is calculated using typical parameter values. The fiber loop length is assumed to be $L = 100$ m. The fiber loss is assumed to be 0.2 dB/km at 1550 nm, and this results in $\alpha = 0.02303\ \text{km}^{-1}$. Two splices are required for the lower path because of the EDFA, whereas one splice is required for the upper path. The splice loss is assumed to be 0.1 dB/splice, and this results in $\varepsilon_1 = 2 \times 0.0115$ and $\varepsilon_2 = 0.0115$. Using these values, the fiber loop loss is given by $\exp[-2\alpha L - 2(\varepsilon_1 + \varepsilon_2)] = 0.93$.

Using the signal-flow graph theory presented in Section 4 and the fiber-optic directional coupler defined in (1), the resulting signal-flow graph representation of the incoherent RPSP is shown in ***Figure 14***.

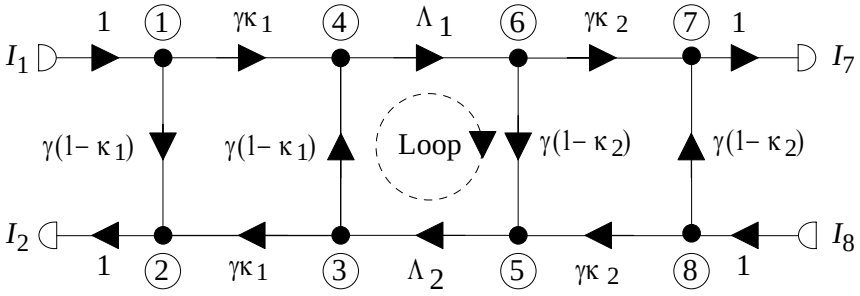

Figure 14 Signal-flow graph representation of the incoherent RPSP. Numbers in circles denote photonic nodes, which correspond to the port numbers of the couplers.

4.2.2Transfer Functions of the Incoherent RPSP

The intensity transfer function I_2/I_1 of the incoherent RPSP is derived in detail. Figure ***Figure 14*** shows that there are two photonic forward paths along which the input signal at node ① can flow to the output node ②. Using Mason's gain formula as defined in (3.5) where $N = 2$, the two photonic forward-path gains can be written as follows:

Path 1: ①→②

$$P_1 = \gamma(1-\kappa_1), \tag{38}$$

***Path 2*:** ①→④→⑥→⑤→③→②

$$P_2 = \gamma^3\kappa_1^2(1-\kappa_2)\Lambda_1\Lambda_2. \tag{39}$$

There is only one photonic loop gain which can be identified as follows:

Loop: ④→⑥→⑤→③→④

$$P_{11} = \gamma^2(1-\kappa_1)(1-\kappa_2)\Lambda_1\Lambda_2. \tag{40}$$

The signal-flow graph determinant is thus given by:

$$D = 1 - P_{11} = 1 - \gamma^2(1-\kappa_1)(1-\kappa_2)\Lambda_1\Lambda_2. \tag{41}$$

The cofactors of the forward paths are:

$$D_1 = D \quad \text{since the forward path 1 does not touch the loop,} \tag{42}$$

$$D_2 = 1 \quad \text{since the forward path 2 touches the loop.} \tag{43}$$

Substituting (41-43) into the Mason's gain, the intensity transfer function I_2/I_1 of the incoherent RPSP can be written as

$$\frac{I_2}{I_1} = \frac{P_1D_1 + P_2D_2}{D} = \frac{\gamma(1-\kappa_1)(1-z_{\text{zero}}z^{-1})}{1-z_{\text{pole}}z^{-1}} \tag{44}$$

where $z = \exp(j\omega T)$ is the well-known z-transform parameter [25] and $T = T_1 + T_2$ is the basic time delay (or sampling period) of the filter. Furthermore, the zero z_{zero} and the system pole z_{pole} in the z-plane are given by

$$z_{\text{zero}} = \frac{\gamma^2(1-2\kappa_1)(1-\kappa_2)G}{(1-\kappa_1)}, \tag{45}$$

$$z_{\text{pole}} = \gamma^2(1-\kappa_1)(1-\kappa_2)G. \tag{46}$$

The intensity transfer function I_7/I_1 can be similarly derived but with less effort than (44). This is because there is only one forward path from the input node ① to the output node ⑦ [i.e., path ①→④→⑥→⑦], and this path also touches the loop. As a result, the cofactor of this path is equal to unity. By inspecting ***Figure 14***, the intensity transfer function I_7/I_1 of the incoherent RPSP can be written simply as

$$I_7/I_1 = \frac{\gamma^2 \kappa_1 \kappa_2 G \exp(-j\omega T_1)}{1 - z_{\text{pole}} z^{-1}} \tag{47}$$

where the numerator corresponds to the photonic forward-path gain. For analytical simplicity, the factor $\exp(-j\omega T_1)$ in (47), which represents the pure propagation delay and only introduces a linear phase term to the phase response, is neglected because it does not alter the essential characteristics of the filter.

It is clear that (47) corresponds to the transfer function of an all-pole photonic filter because the zero is located at the origin. It can thus be stated that:

> *A photonicsignal processor will exhibit the characteristics of an all-pole photonic filter if the forward paths touch all photonic loops in its signal-flow graph representation.*

Based on the above statement, ***Figure 15***(a)–(c) show other possible structures of the all-pole photonic filters with transfer functions Y_2/X_1. Note that they all have only one forward path, which also touches the photonic loop. It is worth mentioning that a single-coupler fiber-optic filter having one loop (or ring) [7], [16] cannot be used as an all-pole photonic filter because there are two forward paths.

The above analysis shows the advantage of the SFG technique over conventional methods because the intensity transfer functions of the incoherent RPSP can be easily derived in a systematic manner. In addition, the technique can identify the property of a particular photonic system.

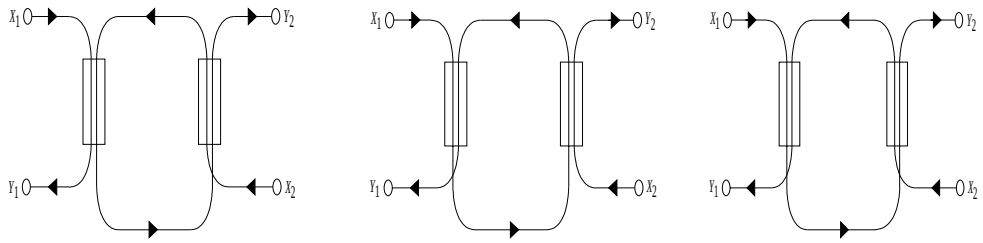

(a) (b) (c)

Figure 15 Schematic diagrams of other possible all-pole photonic filters with transfer functions Y_2/X_1 where $X_2 = 0$.

4.2.3Stability Analysis of the Incoherent RPSP

Stability is one of the most important requirements in the performance of amplified recursive photonic systems in which photonic amplifiers are incorporated. To ensure stable operation of the incoherent RPSP, a first-order system, the system pole must be placed within the unit circle such that the following condition holds:

$$G < \frac{1}{\gamma^2 (1-\kappa_1)(1-\kappa_2)}. \tag{48}$$

The stability of first- and second-order amplified recursive photonic systems can be easily determined because explicit expressions for the system poles can always be obtained. However, it is mathematically involved, if not impossible, to obtain explicit expressions describing the pole locations of third- and higher-order amplified recursive photonic systems, which can be constructed using additional couplers and fiber loops. This difficulty can be overcome using Jury's stability criteria, which has been used with great success for testing the stability of linear time-invariant digital systems [75]. Jury's stability test enables the necessary and sufficient conditions to be obtained, which are usually functions of the system parameters describing the system stability. Binh *et al*. [71] have employed Jury's stability criteria to test the stability of incoherent recursive fiber-optic filters employing photonic amplifiers.

4.2.4Design of the Incoherent RPSP

This section describes two designs of the incoherent RPSP. Desired filtering characteristics of the incoherent RPSP can be obtained by appropriate placement of the pole-zero location in the *z*-plane.

In all designs, the typical value $\gamma = 0.95$ is used. In all figures, the magnitude and phase responses are shown over two frequency cycles which are normalized to $\omega T/(2\pi)$, the time axis of the impulse response represents the time normalized to the basic time delay *T*, and the pole and zero locations in the pole-zero plot are represented by "x" and "o", respectively.

For filter design purposes, it is useful to relate the zero [see (45)] and pole [see (46)] of the intensity transfer function I_2/I_1 according to

$$\frac{z_{\text{pole}}}{z_{\text{zero}}} = \frac{(1-\kappa_1)^2}{(1-2\kappa_1)}. \tag{49}$$

The intensity coupling coefficient of DC1 is determined from (48) to give

$$\kappa_1 = \left[1 - \frac{z_{\text{pole}}}{z_{\text{zero}}}\right] \pm \left\{-\frac{z_{\text{pole}}}{z_{\text{zero}}}\left[1 - \frac{z_{\text{pole}}}{z_{\text{zero}}}\right]\right\}^{1/2} \tag{50}$$

where $$\frac{z_{\text{pole}}}{z_{\text{zero}}} \le 0 \quad \text{or} \quad \frac{z_{\text{pole}}}{z_{\text{zero}}} \ge 1 \tag{51}$$

Equations (46-48) are used to determine the filter parameters required to satisfy a particular prescribed magnitude response.

Design 1: $\mathbf{z_{pole} = 0.99,\quad z_{zero} = -1,\quad \Rightarrow\quad \frac{z_{pole}}{z_{zero}} = -0.99,\quad \Rightarrow\quad \kappa_1 = 0.5864,}$ $\mathbf{\kappa_2 = 0.50,\ G = 5.3.}$

The purpose of this filter design is to design the intensity transfer function I_2/I_1 of the incoherent RPSP with a prescribed magnitude response that has a minima (or notch) at $\omega T = \pi$ and a maxima (or peak) at $\omega T = 2\pi$. This objective can be

accomplished by simultaneously placing the zero near −1 and the system pole near +1.

Figure 16 shows the magnitude, phase and impulse responses and the pole-zero pattern of the intensity transfer function I_2/I_1 of the incoherent RPSP for Design 1. The magnitude response has a minima at the normalized frequency $\omega T/(2\pi) = m + 1/2$ $(m = 0, \pm 1, \pm 2, \cdots)$ because of the zero at $z_{\text{zero}} = -1$, and a maxima at $\omega T/(2\pi) = m$ $(m = 0, \pm 1, \pm 2, \cdots)$ because of the pole at $z_{\text{pole}} = 0.99$. Note that the notches are sharper than the peaks because the zero is located closer to the unit circle than the pole. The magnitude response also shows that the required filter performance is satisfied.

Figure 17 shows that the phase response has sudden phase changes occurring at the minima and maxima frequencies as a result of the computation of the principle value [25]. The periodic characteristics of the magnitude and phase responses are due to the periodic property of the *z*-transform parameter. The decaying characteristics of the intensity impulse response is noted. The intensity impulse response is defined as the response of an incoherent system when excited by a photonicimpulse, which has unity intensity and a coherence time that is very much shorter than the basic time delay *T*. Thus, an intensity impulse response consists of a series of intensity-weighted short photonic pulses separated by the basic time delay. Note that the intensity impulse response is real and positive-valued because of the positive nature of the incoherent (or positive) system [1].

Figure 18 shows the resulting frequency and time responses of the intensity transfer function I_7/I_1 of the incoherent RPSP (or all-pole photonic filter) for Design 1. The maxima of the magnitude response are mainly due to the system pole at $z_{\text{pole}} = 0.99$.

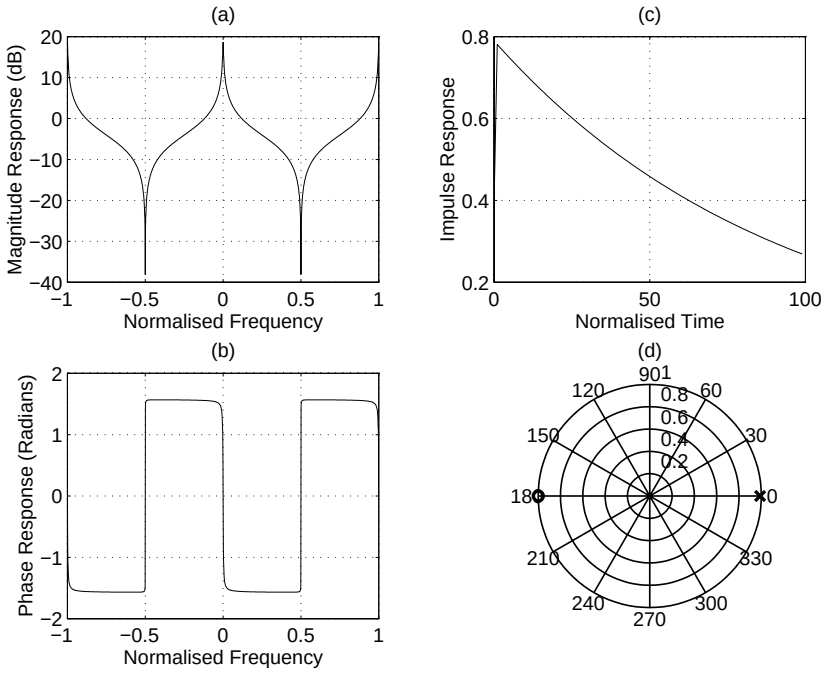

Figure 16 Design 1: Frequency and time responses of the intensity transfer function I_2/I_1 of the incoherent RPSP. (a) Magnitude response. (b) Phase response. (c) Impulse response. (d) Pole-zero patterns.

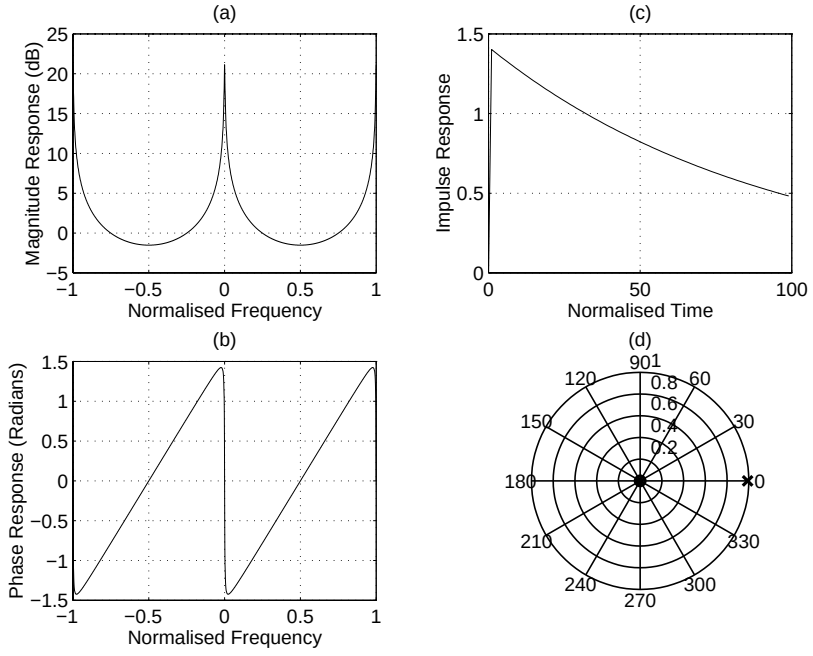

Figure 17 Design 1: Frequency and time responses of the intensity transfer function I_7/I_1 of the incoherent RPSP. (a) Magnitude response. (b) Phase response. (c) Impulse response. (d) Pole-zero patterns.

In summary, the incoherent RPSP having the intensity transfer functions I_2/I_1 and I_7/I_1 can be used as a photonicnarrow-bandpass filter, which can process broadband signals having frequency components at around $\omega T = 2\pi$. In addition, the incoherent RPSP having the intensity transfer function I_2/I_1 can also be used as a photonic notch filter, which can block broadband signals having frequency components at around$\omega T = \pi$.

Design 2: $\mathbf{z_{pole} = 0.05, z_{zero} = -1, \Rightarrow \frac{z_{pole}}{z_{zero}} = -0.05, \Rightarrow \kappa_1 = 0.8209,}$

$\mathbf{\kappa_2 = 0.6745,}$ $\boldsymbol{G = 0.95.}$

The purpose of this filter design is to design the intensity transfer function I_2/I_1 of the incoherent RPSP with a prescribed magnitude response that has a minimum at $\omega T = \pi$. This objective can be accomplished by placing the zero near-1.

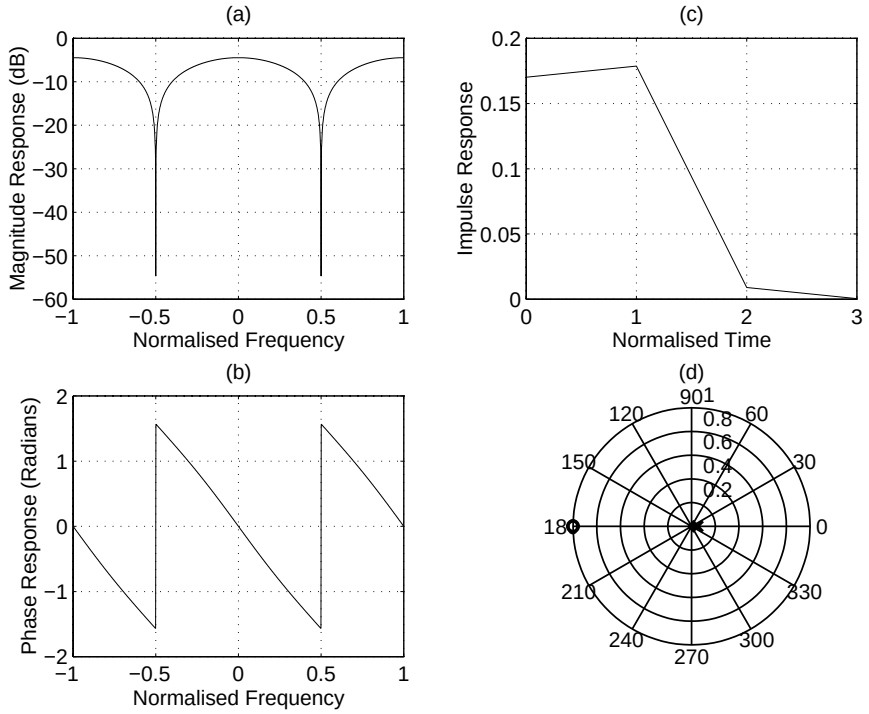

Figure 18 Design 2: Frequency and time responses of the intensity transfer function I_2/I_1 of the incoherent RPSP. (a) Magnitude response. (b) Phase response. (c) Impulse response. (d) Pole-zero patterns.

Figure 18 shows the magnitude, phase and impulse responses and the pole-zero pattern of the intensity transfer function I_2/I_1 of the incoherent RPSP for Design 2.

As would be expected, the minima of the magnitude response occur at $\omega T/(2\pi) = m + 1/2$ $(m = 0, \pm 1, \pm 2, \cdots)$.

Note that the incoherent RPSP cannot be designed to have a magnitude response that has a maxima at $\omega T = \pi$ because the system pole is always positive. In addition, the intensity transfer function I_2/I_1 of the incoherent RPSP cannot be designed to have a minimum at $\omega T = 2\pi$ because its zero is restricted by (49) to take a negative value. Although incoherent fiber-optic signal processors are stable and robust, they can only have certain filtering characteristics, and can only process positive-valued (or intensity-based) signals.

The above designs have shown that the EDFA can compensate for photonic losses as well as providing design flexibility in amplified fiber-optic signal processors [7]. There is an extra degree of freedom in manipulating the pole-zero patterns of amplified systems when compared with non-amplified systems leading to more possible applications of the amplified systems. It is worth pointing out that the incoherent RPSP described here has already been experimentally demonstrated [1], [15], and [76]. The analytical and simulation results presented here, in particular design 1, and are consistent with the experimental results given in reference [15].

4.2.5 Remarks

A framework for the analysis of PSPs through the use of the signal-flow graph method has been presented. The effectiveness of this method has been demonstrated by applying it to derive the intensity transfer functions of the incoherent RPSP. Two designs of the incoherent RPSP and their applications as a photonic narrow-BPF and a photonicnotch filter have also been described. The signal-flow graph technique described in this section is an important mathematical tool in the analysis and design of photonic signal processors throughout this work. The all-pole characteristics of the RPSP are used for the design of photonic processors such as incoherent fiber-optic integrators, the design of a photonic dark-soliton generators and tunable photonic filters.

4.3 Computer Aided Generation of Photonic Transfer Functions[12]

4.3.1Remarks

Determining the behavior of a given photonic circuit has traditionally been done by solving the field (vector) or intensity (scalar) equations for each photonic component simultaneously. This is time consuming and impractical for large circuits; provided some simple requirements are met, a better method using a signal-flow graph approach may be used [5]. The requirements to be satisfied are: (i) Linearity of all photonic components (ii) Time invariance of all photonic components and (iii) Photonic components must be lumped. In other words, we consider only lumped LTIV photonic circuits, either coherent or incoherent operations. Effects such as backscatter of light along the length of a photonicfiber, or saturation of a photonicamplifier are therefore not considered here (the former is a distributed phenomenon, the latter nonlinear). Such circuits may be graphically represented as photonic nodes connected by links. Nodes represent points in the circuit and link the function of the photonic components connecting them. A computer aided generator OPTMASON has been developed for automatic generation of the signal flow of a PSP system. The instruction for using OPTIMASON can be found in the Appendix. The principle of this generator is described in this section.

For example (see ***Figure 19***), consider the following photonic circuit constructed from two 2×2 photonic couplers and some lengths of photonic waveguide:

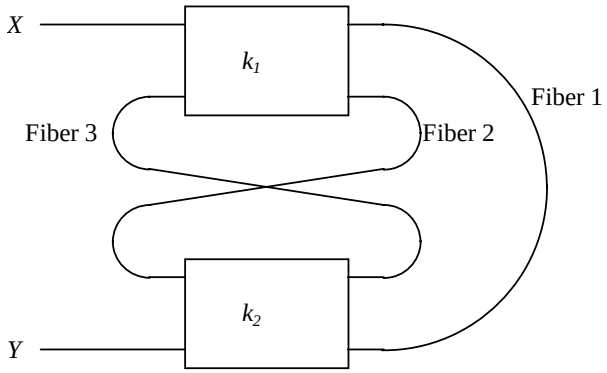

Figure 19 A photonic circuit for automatic generation of transfer function.

[12] see also details in Ref.[80]

Let us assume that there is no coupling between lightwaves propagating along opposite directions in each of the fibers, and that the fibers are symmetrical with respect to the direction of light propagation. Then each fiber may be represented by an expression of the form $t.z^{-L}$ where t is the gain (possibly including a fixed phase factor), L is the length of the fiber, z is the z-transform parameter, $z = exp(j\beta)$ with $\beta = n_f\omega/c$ is the propagation constant of the guided fundamental mode, and n_f is the effective refractive index of that mode (single mode propagation assumed).

The coupling constants of the various ports of the i^{th} 2×2 photonic coupler are as follows: coupling factor $C_i = (1-|k_i|)$ from a port to the port directly opposite coupling factor k_i from a port to the port diagonally opposite. k_i can be imaginary (= $j|k_i|$) if coherent light is being considered, but real if only light intensities are used. The couplers are assumed to be symmetrical. The circuit may then be depicted as follows:

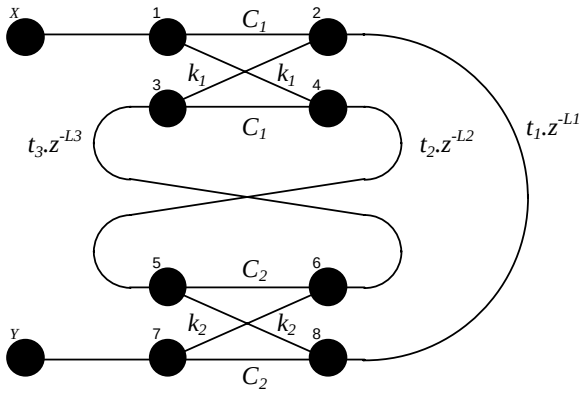

Figure 20 Nodes and photonic transmission paths of a photonic circuit.

This could be called a "*photonic connection graph*". The nodes are represented by dark circles, and the links by lines. Note that this is NOT a signal flow graph: the links depicted here are bi-directional. To create a signal flow graph from the photonic connection graph, it is necessary to double each node and each link, in order to create separate nodes and links for each direction of light propagation. For example

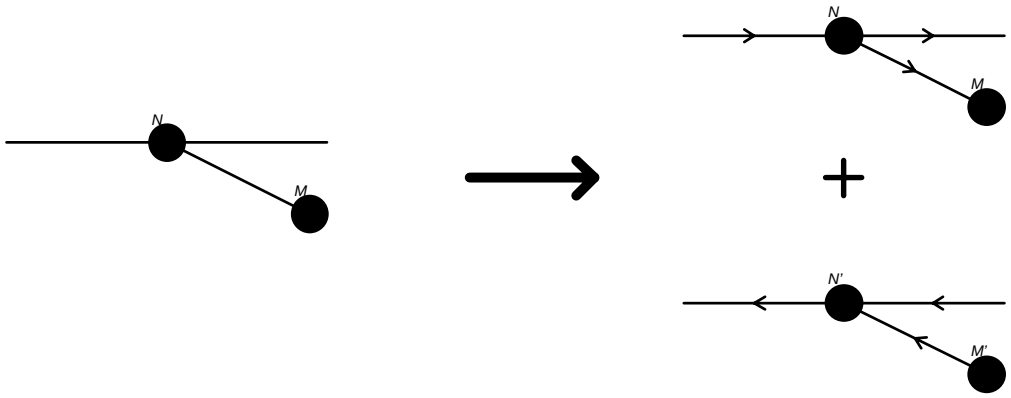

Figure 21: Node and links of bidirectional photonic paths

Once a signal flow graph has been obtained by this doubling method, Mason's rule may be applied to calculate the transfer function between a source node and a sink node (nodes that have only outputs and only inputs respectively; these nodes should not be "doubled"). We take *X* and *Y* above to be the source and sink respectively. Mason's rule depends on the definitions as described in Section 4.

4.3.2OPTMASON: a photonic transfer function generator

OPTMASON is a Borland Pascal program that accepts a text file description of a photonic circuit (in "photonic connection graph" form), and generates its transfer function (from source to sink as specified in the input file). Internally the photonic connection graph is converted into a signal flow graph, and then Mason's rule is applied. The resulting expression is simplified by nested grouping-of-terms.

OPTMASON is written in Borland Pascal (version 7.0). It performs the following basic steps in order to produce the output:

STEP 1: SFG Node geometry

The input file lines $INPUT=… and $OUTPUT=… lines are read, and corresponding input and output (source and sink) nodes are created.

The geometry description section is processed a line at a time. Each new node mentioned in this section actually causes the creation of two nodes (of the same name) in OPTMASON's data structure. Links listed before the semicolon ";" head

out from the first of these, and links listed after the semicolon head out from the second. (NB internally, all links associated with a node are outgoing… that's why the output node does not need a description line). The destination of a link is always to the first node with the correct name. Links to the input node are created to ensure correct operation when the input and output nodes are the same (see (3) below). This stage is complete at the end of the file or when a line starting with "$TRANSMITTANCES" is encountered.

STEP 2: SFG Link Structures

The link structure is checked and adjusted: It is verified that every node (except the sink) has at least one outgoing link, that for each link $n \rightarrow m$ there is a reciprocal link $m \rightarrow n$, and that there is at most one link between any two nodes. The following adjustment is also carried out for each link $n \rightarrow m$: If the two nodes with the name m are denoted m_1 and m_2 then the link is always $n \rightarrow m_1$ at first. If the reciprocal link $m \rightarrow n$ is of the form $m_2 \rightarrow n$ then no action need be taken; but if it is of the form $m_1 \rightarrow n$, then the $n \rightarrow m$ link is adjusted to be $n \rightarrow m_2$. This eliminates all link loops of the form $A \rightarrow B \rightarrow A$, and results in the correct signal flow graph corresponding to the photonic connection graph. This procedure also correctly handles the case where the input and output nodes are the same. (In step (1) it is ensured that the output node precedes the input node in the list of nodes, and so is treated as the first node of that name if the two are the same). If they are not the same, some "phantom" links to the input node will remain, and should be ignored.

STEP 3: SFG Link check

The link value description section is parsed one line at a time, and the link values are set (all are already initialized to 1 at link creation). When a link from a node to itself (i.e. a reflection coefficient) is encountered, it is first checked that one of the two corresponding nodes with that name has NO outputs, then a new link with the desired value is created from that node to its pair node. A check is also done to see whether this link already exists, and if so the value is overwritten rather than a new link created.

STEP 4: Path/Loop Search

A complete depth-first search through the signal flow graph is performed recursively, starting at the input node. When the output node is reached, a new path has been found. An entry in the list of paths is created for it and the path gain is computed. Associated with each node is a list of the paths and the loops that it touches (the "touchpath" and "touchloop" lists respectively). The new path is added to the "touchpath" list of each node along it. Associated with each path is the list of loops that it touches, and to the new path's "touchloop" list is added the contents of each "touchloop" list on each node along the path, checking to ensure that duplicate entries are not made. (NB a path touches any loop that any one of its nodes touches). Similarly, when the search encounters a node that it has been to before a loop has been found. (The last-taken link out of each node is stored during the search, so if this is not nil then the node has been previously traversed. NB this information is also used to follow loops and paths when computing loop/path gain, without disrupting the recursive nature of the search procedure). Associated with each loop is a "touchloop" and a circularly-linked list of nodes in the loop. When a loop has been found, this node list for each loop in the "touchloop" list of the current node is checked, to see if that loop has actually been found before. If not, a new entry for it in the list of loops is created, and *placed at the start of this list*. The loop gain of the new loop is computed (actually -(loop gain), since this is what Mason's rule uses). Also the following is done: (i) A circular node-list for the loop is created (ii) the loop is added to the "touchloop" list of each node along it (iii) the loop is added to the "touchloop" list of each path in the "touchpath" lists of all the nodes along it (iv) the "touchloop" lists of each of the nodes along the new loop are amalgamated (removing duplicate entries) and stored as the "touchloop" list for this loop. Naturally when performing the computations for a new loop or path, they are all done together on a node-by-node basis rather then being completed sequentially as the above descriptions imply. It would be possible to speed up the operation of this stage of OPTMASON by storing the "touchloop" lists in sorted form (or even in binary tree form, etc) to make searching for duplicate entries and list amalgamation more efficient. The lists actually contain pointers, but these could be converted to "longints" for use as sorting keys.

STEP 5: Transmittance Gains for Paths and Loops

When the search is complete, the result is a list of all paths and an ordered list of all loops in the signal flow graph, with their associated pathgains and (-loopgains). Also associated with each path is a list of the loops it touches, and associated with each loop is a list of the paths it touches, and a list of the loops below it in the loop-list that it touches. (That is why the loop list order is important; the loops are in no particular order per se). Since this is all the information Mason's rule requires, all the data associated with each node and link is now deleted to free memory space for further calculation. The node lists for each loop are also deleted.

STEP 6: Mason's denominator

The Mason's rule denominator Δ is calculated. To explain how this is done, it must first be observed that the rule for calculation of Δ given earlier can be expressed as:

Δ = 1+sum of all possible products of (-loopgain) of all nontouching loops.

The list of loops can be regarded as a tree structure: the root node is not a loop, but its branch nodes are each of the loops, and every other node in tree is a loop. Further down the tree, a node has as its branch nodes all loops below it in the list (of loops) that do not touch it or any node above it in the tree. Each possible descent through the tree terminating on an arbitrary node (i.e. not necessarily a leaf node) then represents a unique combination of nontouching loops, and the set descents to all possible nodes in the tree represents the set of all possible combinations of nontouching loops. Δ is calculated, therefore, by a recursive depth-first tree search, which at each node adds to delta the running product of that node's (-loop gain) times the (-loopgains) product of the nodes earlier in the tree, before proceeding to search the branches. Associated with each loop is the number of times it has been "deactivated" or touched by loops along the current descent path. The search works by simply searching all loops below the current tree-node in the loop-list that have not been deactivated (touched) yet.

STEP 7: Mason's gain numerator

The Mason's rule numerator is calculated. This involves stepping through each path in turn and adding to the numerator the path gain times Δ_k for that (the k^{th}) path. Δ_k is calculated the same way Δ is, but the loops touching the current (k^{th}) path are first given a "deactivation level" of 1 so they will not be included.

STEP 8: Alphabetical transfer function

The results are outputted (in symbolic form) either to the screen (DOS standard re-directable output) or to the specified output file (appending it if it is the same as the input file). All dynamic variables are then disposed of before the program completes execution.

The above functions account for approximately 2/3 of the OPTMASON listing. The other 1/3 of the program is devoted to manipulating the symbolic expressions that result from calculations on link values and on path and loop gains.

OPTMASON expressions are stored in a hierarchical tree-like structure, and all operations on them are performed recursively. The structure corresponding to an expression is built up out of records of type "expression_type". A "format" field in each of these records identifies it as belonging to one of four possible types:

- *A "zterm" - a term of the form* $z^{num*\{expr\}}$. *If expr is absent (nil pointer) then it just represents* z^{num}.
- *An "anglterm" - a term of the form exp(j.num.{expr}). If expr is absent, just exp(j.num).*
- *A "magterm" - a term of the form* $\{expr\}^{num}$.
- *A "magval" - a real number, = num.*

In all the above cases "num" is a double-precision real number, and "expr" is a string representing a variable or a mathematical expression; it is what appears inside {} brackets in the input file. No processing is performed on the *contents* of expr. (Actually expr^, since expr is a pointer to the string).

Apart from the "format", "num", and "expr" fields, expression_type also has "sumterm" and "prodterm" field, which point to other expression records, or are nil. They define the structure of a mathematical expression. This is best illustrated

graphically: horizontal arrows represent the sumterm pointers, vertical arrows the prodterm pointers, and the absence of an arrow indicates that that pointer is nil. Each letter below represents a single term, i.e. single expression_type record.

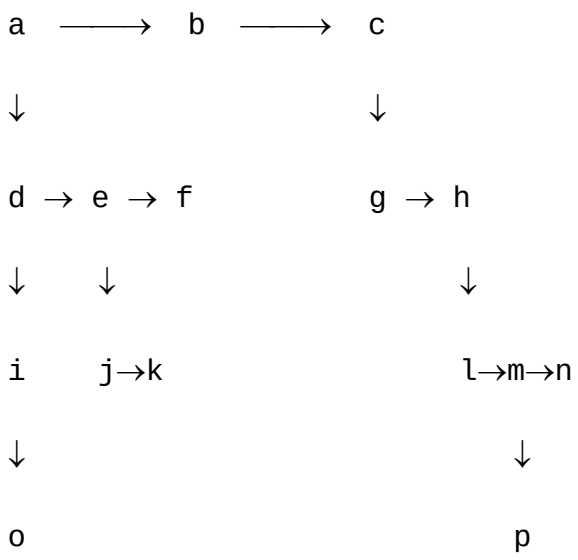

This entire structure corresponds to the expression:

$$(o.i.d+(j+k)e+f)a + b + (g+(l+p.m+n)h)c$$

A boolean function precedes(x,y) is used to determine if the term x "precedes" the term y. Order of precedence is as follows: zterm < anglterm < magterm < magval. If x and y are of the same format, then ascii comparison of $\{expr\}_x$ and $\{expr\}_y$ is used to decide whether x precedes y, and if these are equal, num_x is compared to num_y. The precedes() function always returns "true" if x=y, or if they are both "magval"s (so it should really be called "equal_or_precedes").

The expression tree for an expression is ordered so that if a term x contains a link to a term y (either sumterm or prodterm link), then precedes(x,y) will be true. This has the effect of bringing "zterm"s outside of brackets, and summing "magval"s and "magterm"s together inside brackets - which hopefully results in the most compact and legible output.

"Magval"s are thus the leaves of the expression tree. A nil pointer in an expression or to an expression is treated as a zero. Thus, if a prodterm pointer is nil, the terms it

multiplies get canceled. The exception is on “magval” terms, which must therefore terminate every path down through the tree; a nil prodterm pointer is required on “magval” type terms.

Addition of one expression to another is performed as follows: Each term in the top-level sum list (i.e. root, root^.sumterm, root^.sumterm^.sumterm… etc) of the expression being added is compared with each successive term of the top-level sum list of the expression being added to, until the term being added is found to precede() the term it is compared to. If they are addable - which occurs if they are equal or both magvals - then if they are magvals the value of the term being added is just added; otherwise, the addition procedure is called recursively to add their prodterm subexpressions (since ax+bx = (a+b)x). If they are not addable, then the term being added is simply inserted into the top-level sum list of the expression being added to, along with the subexpression pointed to by its prodterm… i.e. along with anything multiplying it.

Multiplication is performed in a similar manner: to create a new expression that is the product of two others, the product expression is set to zero, then every term in the top-level sum list of the first is compared with every term in the top-level sum list of the other. If a pair of such terms can be multiplied directly (i.e. if they are both “magval”s or if they are of the same format and have the same {expr}) then this is done, and both their prodterm subexpressions are multiplied (calling the multiply procedure recursively). Otherwise the prodterm subexpression of the “precede()”ing term is multiplied (recursively) by the other term and its product subexpression. In either case, the result is added to the final product (using the addition procedure described above).

Due to the regular sorted (by the precedes () function) way in which expressions are stored and manipulated, they are automatically simplified by grouping of terms at every stage in the calculation. This is not only efficient, but almost certainly necessary for handling the huge sum-of-product type expressions that might result from calculation of the Mason’s rule Δs for large graphs if simplification were not used, without running out of memory.

Finally, the procedure used to output expressions works in a similar manner as those used to manipulate them: Each top-level sum term is handled in turn, first outputting the prodterm subexpression (by calling the output routine recursively), then outputting the term it multiplies, and a "+" if more sumterms remain. At least, that's how it works in principle: In practice, there are exceptions and modifications. In particular, when "+" needs to be output, it is not done right away, but a plus_waiting flag is set instead. Then, when the next item is outputted, the waiting "+" is outputted first, *unless then next item to be outputted begins with a minus sign*. This eliminates output of the form x+-6y. Similarly, checks are made for multiplication by +/-1 to avoid outputting the numeral. "prodterm" subexpressions involving sums are bracketed, and those that do not are not. An {expr} part of a term that is treated as a single variable (see above) will not have brackets around it, otherwise it will be enclosed in [] brackets, except when it appears in a sum nothing except +1 multiplying it. "prodterm" subexpressions are in general outputted recursively, but where products of multiple single zterms or single anglterms occur, the entire product is displayed within a single z^(…+…) or exp(j(…+…)) to make the output easier to read; recursion is not used in this case, and the product list is stepped through manually until an incompatible term is found (i.e. that cannot be put within the same brackets).

5 Concluding Remarks

The new field of photonic signal processing is proposed. Part I gives an illustration of how a simple photonic circuit can be presented with the signal flow and processing the lightwaves with the relationship between input ports and output ports. The photonic transfer functions can be then derived, manually or automatically, so that their amplitude and phase characteristics can be obtained.

A number of photonic components have been illustrated and represented with the gain/loss and propagation delay factors in forms of the z-transform parameters that would allow the applications of popular digital signal processing techniques. Future reports will present the design and synthesis of several photonic processors in 1-D. Proposed techniques for multi-D PSP systems have been reported [78]. This report thus sets the initial steps for the series on photonic signal processing.

6 Acknowledgement

The author wishes to acknowledge the contributions of some parts of this report which were developed by Ngo Quoc Nam while he was a PhD candidate at Monash university [79].

7 References

[1] B. Moslehi, J. W. Goodman, M. Tur, and H. J. Shaw, "Fiber-optic lattice signal processing," *Proc. IEEE*, vol. 72, pp. 909–930, 1984.
[2] K. P. Jackson, S. A. Newton, B. Moslehi, M. Tur, C. C. Cutler, J. W. Goodman, and H. J. Shaw, "Photonic fiber delay-line signal processing," *IEEE Trans. Microwave Theory and Techniques*, vol. MTT-33, pp. 193–210, 1985.
[3] C. C. Wang, "High-frequency narrow-band single-mode fiber-optic transversal filters," *J. Lightwave Technol.*, vol. LT-5, pp. 77–81, 1987.
[4] R. I. MacDonald, "Switched photonic delay-line signal processors," *J. Lightwave Technol.*, vol. LT-5, pp. 856–861, 1987.
[5] D. M. Gookin and M. H. Berry, "Finite impulse response filter with large dynamic range and high sampling rate," *Appl. Opt.*, vol. 29, pp. 1061–1062, 1990.
[6] A. Ghosh and S. Frank, "Design and performance analysis of fiber-optic infinite-impulse response filters," *Appl. Opt.*, vol. 31, pp. 4700–4711, 1992.
[7] B. Moslehi, "Fiber-optic filters employing photonic amplifiers to provide design flexibility," *Electron. Lett*., vol. 28, pp. 226–228, 1992.
[8] B. Moslehi and J. W. Goodman, "Novel amplified fiber-optic recirculating delay line processor," *J. Lightwave Technol.*, vol. 10, pp. 1142–1147, 1992.
[9] B. Moslehi, K. K. Chau, and J. W. Goodman, "Photonic amplifiers and liquid-crystal shutters applied to electrically reconfigurable fiber optic signal processors," *Opt. Eng.*, vol. 32, pp. 974–981, 1993.
[10] J. Capmany and J. Cascon, "Photonic programmable transversal filters using fiber amplifiers," *Electron. Lett*., vol. 28, pp. 1245–1246, 1992.
[11] J. Capmany and J. Cascon, "Discrete time fiber-optic signal processors using photonic amplifiers," *J. Lightwave Technol.*, vol. 12, pp. 106–117, 1994.
[12] S. Sales, J. Capmany, J. Marti, and D. Pastor, "Solutions to the synthesis problem of photonic delay line filters," *Opt. Lett.*, vol. 20, pp. 2438–2440, 1995.
[13] S. Sales, J. Capmany, J. Marti, and D. Pastor, "Novel and significant results on the non-recirculating delay line with a fiber loop," *IEEE Photon. Technol. Lett.*, vol. 7, pp. 1439–1440, 1995.
[14] S. Sales, D. Pastor, J. Capmany, and J. Marti, "Fiber-optic delay-line filters employing fiber loops: signal and noise analysis and experimental characterization," *J. Opt. Soc. Am. A*, vol. 12, pp. 2129–2135, 1995.
[15] D. Pastor, S. Sales, J. Capmany, J. Marti, and J. Cascon, "Amplified double coupler fiber-optic delay line filter," *IEEE Photon. Technol. Lett.*, vol. 7, pp. 75–77, 1995.
[16] M. C. Vazquez, B. Vizoso, M. Lopez-Amo, and M. A. Muriel, "Single and double amplified recirculating delay lines as fiber-optic filters," *Electron. Lett*., vol. 28, pp. 1017–1019, 1992.

[17] M. C. Vazquez, R. Civera, M. Lopez-Amo, and M. A. Muriel, "Analysis of double-parallel amplified recirculating photonic-delay lines," *Appl. Opt.*, vol. 33, pp. 1015–1021, 1994.
[18] C. Vazquez, M. Lopez-Amo, M. A. Muriel, and J. Capmany, "Performance parameters and applications of a modified amplified recirculating delay line," *Fiber and Integrated Optics*, vol. 14, pp. 347–358, 1995.
[19] B. Vizoso, C. Vazquez, R. Civera, M. Lopez-Amo, and M. A. Muriel, "Amplified fiber-optic recirculating delay lines," *J. Lightwave Technol.*, vol. 12, pp. 294–305, 1994.
[20] B. Vizoso, I. R. Matias, M. Lopez-Amo, M. A. Muriel, and J. M. Lopez-Higuera, "Design and application of double amplified recirculating ring structure for hybrid fiber buses," *Opt. and Quantum Electron.*, vol. 27, pp. 847–857, 1995.
[21] E. C. Heyde and R. A. Minasian, "A solution to the synthesis problem of recirculating photonic delay line filters," *IEEE Photon. Technol. Lett.*, vol. 6, pp. 833–835, 1994.
[22] E. C. Heyde, "Theoretical methodology for describing active and passive recirculating delay line systems," *Electron. Lett.*, vol. 31, pp. 2038–2039, 1995.
[23] J. Capmany, J. Cascon, J. L. Martin, S. Sales, D. Pastor, and J. Marti, "Synthesis of fiber-optic delay line filters," *J. Lightwave Technol.*, vol. 13, pp. 2003–2012, 1994.
[24] S. Sales, J. Capmany, J. Marti, and D. Pastor, "Experimental demonstration of fiber-optic delay line filters with negative coefficients," *Electron. Lett.*, vol. 31, pp. 1095–1096, 1995.
[25] A. V. Oppenheim and R. W. Schafer, *Discrete-time signal processing*, Englewood Cliffs, NJ: Prentice-Hall, 1989.
[26] G. P. Agrawal, *Fiber-optic communication systems*, John Wiley and Sons, 1992.
[27] S. K. Sheem and T. G. Giallorenzi, "Single-mode fiber-photonic power divider: Encapsulated etching technique," *Opt. Lett.*, vol. 4, pp. 29–31, 1979.
[28] M. J. F. Digonnet and H. J. Shaw, "Analysis of a tunable single mode photonic fiber coupler," *IEEE J. Quantum Electron.*, vol. QE-18, pp. 746–754, 1982.
[29] S. Shimada and H. Ishio, eds., *Photonic amplifiers and their applications*, John Wiley and Sons, 1994, chapters 1–5.
[30] J. C. Cartledge and G. S. Burley, "The effect of laser chirping on lightwave system performance," *J. Lightwave Technol.*, vol. 7, pp. 568–573, 1989.
[31] S. E. Miller, "Integrated optics: an introduction," *Bell Syst. Tech. J.*, vol. 48, pp. 2059–2069, 1969.
[32] T. Tamir, ed., *Integrated optics*, Springer-Verlag: New York, 1975.
[33] L. D. Hutcheson, *Integrated photonic circuits and components*, Marcel Dekker: New York, 1987.
[34] S. E. Miller and I. P. Kaminow, eds., *Photonic fiber telecommunications II*, Academic Press, 1988.
[35] R. G. Hunsperger, *Integrated optics: theory and technology*, Springer-Verlag: New York, third edition, 1991.
[36] J. M. Senior, *Photonic fiber communications: principles and practice*, Prentice Hall: London, second edition, 1992.
[37] M. Kawachi, "Silica waveguides on silicon and their application to integrated-optic components," *Opt. and Quantum Electron.*, vol. 22, pp. 391–416, 1990.

[38] M. Kawachi, "Recent progress in planar lightwave circuits," *10th International Conf. Integrated Optics and Photonic Fiber Commun.*, Hong Kong, *Proc. IOOC'95*, vol. 3, pp. 32–33, 1995.
[39] C. H. Henry, "Silica planar waveguides," *Proc. IREE, 19th Australian Conf. Opt. Fiber Technol.*, Melbourne, pp. 326–328, 1994.
[40] B. H. Verbeek, C. H. Henry, N. A. Olsson, K. J. Orlowsky, R. F. Kazarinov, and B. H. Johnson, "Integrated four-channel Mach-Zehnder multi/demultiplexer fabricated with phosphorous doped SiO_2 waveguides on Si," *J. Lightwave Technol.*, vol. 6, pp. 1011–1017, 1988.
[41] T. Kitoh, N. Takato, K. Jinguji, M. Yasu, and M. Kawachi, "Novel broad-band photonic switch using silica-based planar lightwave circuit," *IEEE Photon. Technol. Lett.*, vol. 4, pp. 735–737, 1992.
[42] M. Okuno, K. Kato, Y. Ohmori, M. Kawachi, and T. Matsunaga, "Improved 8×8 integrated photonic matrix switch using silica-based planar lightwave circuits," *J. Lightwave Technol.*, vol. 12, pp. 1597–1606, 1994.
[43] R. Nagase, A. Himeno, M. Okuno, K. Kato, K. Yukimatsu, and M. Kawachi, "Silica-based 8×8 photonic matrix switch module with hybrid integrated driving circuits and its system application," *J. Lightwave Technol.*, vol. 12, pp. 1631–1639, 1994.
[44] Y. Hida, N. Takato, and K. Jinguji, "Wavelength division multiplexer with passband and stopband for$1.3\mu m / 1.55\mu m$ using silica-based planar lightwave circuit," *Electron. Lett*., vol. 31, pp. 1377–1379, 1995.
[45] K. Okamoto, K. Takiguchi, and Y. Ohmori, "16-channel photonic add/drop multiplexer using silica-based array-waveguide gratings," *Electron. Lett*., vol. 31, pp. 723–724, 1995.
[46] K. Okamoto, M. Ishii, Y. Hibino, Y. Ohmori, and H. Toba, "Fabrication of unequal channel spacing array-waveguide grating multiplexer modules," *Electron. Lett*., vol. 31, pp. 1464–1465, 1995.
[47] K. Sasayama, M. Okuno, and K. Habara, "Photonic FDM multichannel selector using coherent photonic transversal filter," *J. Lightwave Technol.*, vol. 12, pp. 664–669, 1994.
[48] K. Oda, S. Suzuki, H. Takahashi, and H. Toba, "A photonicFDM distribution experiment using a high finesse waveguide-type double ring resonator," *IEEE Photon. Technol. Lett.*, vol. 6, pp. 1031–1034, 1994.
[49] S. Suzuki, M. Yanagisawa, Y. Hibino, and K. Oda, "High-density integrated planar lightwave circuits using $\underline{SiO_2 - GeO_2}$ waveguides with a high-refractive index difference," *J. Lightwave Technol.*, vol. 12, pp. 790–796, 1994.
[50] S. Suzuki, K. Oda, and Y. Hibino, "Integrated-optic double-ring resonators with a wide free spectral range of 100 GHz," *J. Lightwave Technol.*, vol. 13, pp. 1766–1771, 1995.
[51] E. Pawlowski, K. Takiguchi, M. Okuno, K. Sasayama, A. Himeno, K. Okamato, and Y. Ohmori, "Variable bandwidth and tunable centre frequency filter using transversal-form programmable photonic filter," *Electron. Lett*., vol. 32, pp. 113–114, 1996.
[52] K. Okamoto, M. Ishii, Y. Hibino, and Y. Ohmori, "Fabrication of variable bandwidth filters using arrayed-waveguide gratings," *Electron. Lett*., vol. 31, pp. 1592–1594, 1995.

[53] K. Takiguchi, K. Jinguji, K. Okamato, and Y. Ohmori, "Dispersion compensation using a variable group-delay dispersion equaliser," *Electron. Lett*., vol. 31, pp. 2129–2194, 1995.
[54] K. Takiguchi, S. Kawanishi, H. Takara, K. Okamato, K. Jinguji, and Y. Ohmori, "Higher order dispersion equaliser of dispersion shifted fiber using a lattice-form programmable photonic filter," *Electron. Lett*., vol. 32, pp. 755–757, 1996.
[55] C. H. Henry, G. E. Blonder, and R. F. Kazarinov, "Glass waveguides on silicon for hybrid photonic packaging," *J. Lightwave Technol.*, vol. 7, pp. 1530–1539, 1989.
[56] Y. Yamada, A. Takagi, I. Ogawa, M. Kawachi, and M. Kobayashi, "Silica-based photonic waveguide on terraced silicon substrate as hybrid integration platform," *Electron. Lett*., vol. 29, pp. 444–446, 1993.
[57] S. Mino, K. Yoshino, Y. Yamada, M. Yasu, and K. Moriwaki, "Optoelectronic hybrid integrated laser diode module using planar lightwave circuit platform," *Electron. Lett*., vol. 30, pp. 1888–1890, 1994.
[58] E. E. L. Friedrich, M. G. Oberg, B. Broberg, S. Nilsson, and S. Valette, "Hybrid integration of semiconductor lasers with Si-based single-mode ridge waveguides," *J. Lightwave Technol.*, vol. 10, pp. 336–339, 1992.
[59] Y. Yamada, H. Terui, Y. Ohmori, M. Yamada, A. Himeno, and M. Kobayashi, "Hybrid-integrated 4×4 photonic gate matrix switch using silica-based photonic waveguides and LD array chips," *J. Lightwave Technol.*, vol. 10, pp. 383–390, 1992.
[60] G. Nykolak, M. Haner, P. C. Becker, J. Shmulovich, and Y. H. Wong, "Systems evaluation of an Er^{3+} – doped planar waveguide amplifier," *IEEE Photon. Technol. Lett.*, vol. 5, pp. 1185–1187, 1993.
[61] K. Hattori, T. Kitagawa, M. Oguma, Y. Ohmori, and M. Horiguchi, "Erbium-doped silica-based waveguide amplifier integrated with a 980 / 1530 nm WDM coupler," *Electron. Lett*., vol. 30, pp. 856–857, 1994.
[62] R. N. Ghosh, J. Shmulovich, C. F. Kane, M. R. X. de Barros, G. Nykolak, A. J. Bruce, and P. C. Becker, "8-mW threshold Er^{3+} – doped planar waveguide amplifier," *IEEE Photon. Technol. Lett.*, vol. 8, pp. 518–520, 1996.
[63] K. Takiguchi, K. Okamoto, Y. Inoue, M. Ishii, K. Moriwaki, and S. Ando, "Planar lightwave circuit dispersion equalizer module with polarization insensitive properties," *Electron. Lett.*, vol. 31, pp. 57–58, 1995.
[64] N. Takato, K. Jinguji, M. Yasu, H. Toba, and M. Kawachi, "Silica-based single-mode waveguides on silicon and their application to guided-wave photonic interferometers," *J. Lightwave Technol.*, vol. 6, pp. 1003–1010, 1988.
[65] K. Oda, N. Takato, H. Toba, and K. Nosu, "A wide-band guided-wave periodic multi/demultiplexer with a ring resonator for photonic FDM transmission systems," *J. Lightwave Technol.*, vol. 6, pp. 1016–1023, 1988.
[66] N.Q. Ngo, L.N. Binh, and X. Dai, "Photonic dark-soliton generators and detectors," *Optics Communications*, vol. 132, pp. 389–402, 1996.
[67] K. Oda, N. Takato, and H. Toba, "A wide-FSR waveguide double-ring resonator for photonic FDM transmission systems," *J. Lightwave Technol*., vol. 9, pp. 728–736, 1991.
[68] S. J. Mason, "Feedback theory-some properties of signal flow graphs," *Proc. IRE*, vol. 41, pp. 1144–1156, 1953.
[69] S. J. Mason, "Feedback theory-further properties of signal flow graphs," *Proc. IRE*, vol. 44, pp. 920–926, 1956.

[70] L. N. Binh, N. Q. Ngo, and S. F. Luk, "Graphical representation and analysis of the Z-shaped double-coupler photonic resonator," *J. Lightwave Technol.*, vol. 11, pp. 1782–1792, 1993.
[71] L. N. Binh, S. F. Luk, and N. Q. Ngo, "Amplified double-coupler double-ring photonic resonators with negative photonic gain," *Appl. Opt.*, vol. 34, pp. 6086–6094, 1995.
[72] L. N. Binh, X. T. Nguyen, and N. Q. Ngo, "Realisation of Butterworth-type photonic filters using phase modulators and 3×3 coupler ring resonators," *IEE Proc.-Optoelectron.*, vol. 143, pp. 126–134, 1996.
[73] L. P. A. Robichaud, M. Boisvert, and J. Robert, *Signal flow graphs and applications*, Englewood Cliffs, N.J.: Prentice-Hall, 1962.
[74] J. J. Distefano, A. R. Stubberud, and I. J. Williams, *Theory and problems of feedback and control systems*, Singapore: McGraw-Hill, ch. 8, 1987.
[75] B. C. Kuo, *Digital control systems*, New York: Reinhart & Winston, ch. 5, 1980.
[76] J. E. Bowers, S. A. Newton, W. V. Sorin, and H. J. Shaw, "Filter response of single-mode fiber recirculating delay lines," *Electron. Lett.*, vol. 18, pp. 110–111, 1982.
[77] H. J. Caufield, W. T. Rhodes, M. J. Foster, and S. Horvitz, "Photonic implementation of systolic array processing," *Optics Communications*, vol. 40, pp. 86–90, 1981.
[78] See for examples: L.N. Binh et alia., http://www.ds.eng.monash.edu.au/techrep/reports/2005/MECSE-6-2005.pdf and other reports of the same website: http://www.ds.eng.monash.edu.au/techrep/reports.
[78] L.N. Binh, "Multi-dimensional Photonic Signal Processing" http://www.ds.eng.monash.edu.au/techrep/reports/2005/MECSE-1-2005.pdf, January 2005.
[79] Ngo, Q.N., "New Photonic Signal Processors: Design and Application to Photonic Computing and Photonic Communication systems", PhD dissertation, Monash university, 1997.
[80 LN Binh and D. Trower, "O*PTMASON: A program for AUTOMATIC DERIVATION of the optical transfer functions of PHOTONIC CIRCUITS from their connection graphs"* http://www.ds.eng.monash.edu.au/techrep/reports/2004/MECSE-34-2004.pdf

8 APPENDIX: Using "OPTIMASON" The Computer Aided Generator

OPTMASON is started from the DOS command line by typing:

```
optmason input_file [output_file] [-d]
```

here "input_file" and "output_file" are the corresponding filenames, and "d" is the number of decimal places to display real numbers to in the output; if omitted, "d" defaults to 3. If the output filename is omitted, output is to the screen (actually to DOS's standard output file, to enable redirection). If the input and output filenames are the same, the input file is not overwritten, but is instead appended (i.e. OPTMASON's output is added to the end of it).

The input text file format for OPTMASON is as follows:

$INPUT = *nodename*
$OUTPUT = *nodename*
nodename: *nodename, nodename,…* ; *nodename, nodename,…*
nodename: *nodename, nodename,…* ; *nodename, nodename,…*
nodename: *nodename, nodename,…* ; *nodename, nodename,…*
$TRANSMITTANCES
[*]*nodename, nodename = expression*
[*]*nodename, nodename = expression*
[*]*nodename, nodename = expression*

Here *nodename* is a label for a node of the photonic connection graph. It may be any string of up to 15 characters, but not containing any of the characters "`;:,=$*`" (double quotes are OK though). e*xpression* is a mathematical expression (see below).

The first line ($INPUT=…) identifies the input (source) node.

The second line ($OUTPUT=…) identifies the output (sink) node.
The input and output nodes may be the same node.
The next section defines the geometry of the photonic connection graph.
A line of the form
nodename: *nodename, nodename,…* ; *nodename, nodename,…*

is required for each node in the graph except the output node. (If a line for the output node is included, it will be ignored, unless that node is also the input node.)

Each such line begins with the name of the node being defined, followed by a colon ":". The remainder of the line is a list of all the other nodes that it connects to. Since light may travel independently in two directions through a node in a photonicconnection graph, connections on either "side" (photonically speaking) are separated by a semicolon ";". The definition for the input node and any node at the free end of a photonicwaveguide (reflection point) will only include one "side" of this list.

Since links in a photonic connection graph are bi-directional, a link from *n to m* in the definition of a node *n* must be matched by a corresponding link from *m to n* in the definition of node *m*; links to the output node are an exception. NOTE *that only a single link may join any two nodes*. For multiple photonic paths between two nodes, intermediate nodes must be inserted.

The geometry definition section is terminated by the "$TRANSMITTANCES" line.

The section following this line defines the values of the links in the photonic connection graph. Since all links have a default value of unity in both directions, only the values of links that differ from this need be defined. The format for specifying the value of a link between two nodes *n and m* (value given by "*expression*") is:

n,m = *expression*

To define the value of the link in the direction n → m only, place an asterix "*" at the start of the line. Note that if a link value is defined twice, the second definition replaces the first (both directions are treated independently).

To define the reflection coefficient at a node r, simply write:

r,r = *expression*

An asterix "*" is optional and has no effect. Reflection coefficients may ONLY be defined at nodes that are photonically single-sided (e.g. cut-end of a photonicfiber), and may not be defined for the input or output nodes.

Some other things to note about the input file format are:

- The input is case-sensitive for node names and variables within expressions.
- Whitespace (spaces, tabs, and blank lines) are ignored or filtered out.
- The start of the file is ignored up to the line starting with "$INPUT=" so it may be used for a description of the file contents.
- Any line beginning with a semicolon ";" is treated as a comment and ignored.
- Input lines will be truncated beyond 255 characters.

"*expression*"s have the following form:

***magnitude* {*mag_expr*} ^*power* < *angle* {*angle_expr*} z ^*power* {*power_expr*}**

magnitude, *angle*, and *power* are real numbers (scientific notation, e.g. -1.2e+7 is permitted).

"z" may be uppercase or lowercase (the z-transform parameter).

mag_expr, *angle_expr*, *power_expr* may be any strings at all provided they do not contain "}". They are intended to be variable names or entire subexpressions.

Any part or parts of the above expression format may be omitted, provided that a meaningful expression results. The following are examples of valid expressions and their corresponding mathematical meaning:

6	= 6
2.96E-9{*a*}^2	= $2.96\times10^{-9}\,a^2$
< {pi.beta}	= exp(*j*(pi.beta))
-3 < 1.2	= -3exp(*j*1.2)
Z^-4{L}	= z^{-4L}
-5.2{x*y/z}^3 < 6.4{beta.pi} z^{L+n}	=-.2(x*y/z)^{3}exp(*j*.6.4(beta.pi))$z^{(L+n)}$

Note that although parts of the expression format may be omitted, the ordering of expression components must be strictly adhered to. Also:

- The first "^*power*" is a power of "*mag_expr*" and may only be present if "*mag_expr*" is also.
- The second "*power*" and "*power_expr*" apply to the "z", so can only be present if it is also.
- A single "-" sign is not a number, and cannot precede any of the {} brackets on its own. Use -1{…} to obtain the same effect.
- Expressions in {} brackets are not simplified internally; they are treated as single variables. However when displaying the output, OPTMASON distinguishes two classes of {} expression:

(1) A string inside {} brackets is treated as a single variable if it is composed only of letters, numbers, and the characters "~#@$%?_", and if it does not begin with a digit (0-9). It may also end with a string of single quotes " ' ". As a single variable, it will appear in summations, products, and power expressions *without brackets around it*. So for correct output, products of two variables contained within {} should include a "." or "*" symbol. e.g. if $t_2\,x$ is a product, entering {t2x} may result in the output containing (say) t2x^3 which looks like $t_2\,x^3$ when what is desired is $(t_2\,x)^3$.

(2) Any other string inside {} brackets will appear bracketed in the output. In particular, any string containing any of the mathematical symbols "[](){}+-*./^<>=!" will appear bracketed (inside square brackets) in the output except if it appears on its own (without any multiplying terms) in a summation.

Here are the contents of the input file for the example given earlier:

```
This file is an example of an input file for the sample network
included
in the OPTMASON documentation.
The next two lines define the names of the input (source) and
output (sink)
nodes:
$INPUT = X
$OUTPUT = Y
; The transfer function calculated by OPTMASON will be T = Y/X
; Here is a description of the network geometry:
X:      1
1:      X    ;  2,4
```

```
 2:      1,3  ;  8
 3:      6    ;  2,4
4:      1,3  ;  5
5:      4    ;  6,8
6:      5,7  ;  3
7:      Y    ;  6,8
8:      5,7  ;  2
; not necessary, but included for completeness:
Y:      7
$TRANSMITTANCES
; Internal photonic coupler transmittances:
1,2 = {C1} ; 3,4 = {C1} ; 1,4 = {k1} ;2,3 = {k1}; 5,6 = {C2};
7,8 = {C2}; 5,8 = {k2}; 6,7 = {k2};
;  We  ignore  the  links  from  X  and  Y  because  they  don't
contribute to the magnitude response of the system, or affect
its pole and zero positions.
; ...so they default to values of 1.
; The three main photonic fiber transmittances:
2,8 = {t1} z^-1{L1}
4,5 = {t2} z^-1{L2}
3,6 = {t3} z^-1{L3}
; Thats all we need! (simple, isn't it?)
```

Here is OPTMASON's output:

```
T = numerator/denominator
numeratorá=á((k1^2+C1^2)*k2^2+C2^2*k1^2-2*C1^2*C2^2)*t1*t2*t3*z
^(-L3-L2-L1)+((C1*C2*k1^2-C1^3*C2)*k2^2-C1*C2^3*k1^2+C1^3*C2^3)
*t1*t2^2*t3^2*z^(-2*L3-2*L2-L1)+C1*C2*t1*z^-L1
denominator              =              -2*C1*C2*t2*t3*z^(-L3-
L2)+C1^2*C2^2*t2^2*t3^2*z^(-2*L3-2*L2)+1
```